J. Fluid Mech. (2002), *vol.* 451, *pp.* 109–144.
DOI: 10.1017/S002211200100636X Printed in the United Kingdom

A numerical investigation of solitary internal waves with trapped cores formed via shoaling

By KEVIN G. LAMB

Department of Applied Mathematics, University of Waterloo,
Waterloo, Ontario, Canada N2L 3G1

(Received 11 August 1999 and in revised form 28 June 2001)

The formation of solitary internal waves with trapped cores via shoaling is investigated numerically. For density fields for which the buoyancy frequency increases monotonically towards the surface, sufficiently large solitary waves break as they shoal and form solitary-like waves with trapped fluid cores. Properties of large-amplitude waves are shown to be sensitive to the near-surface stratification. For the monotonic stratifications considered, waves with open streamlines are limited in amplitude by the breaking limit (maximum horizontal velocity equals wave propagation speed). When an exponential density stratification is modified to include a thin surface mixed layer, wave amplitudes are limited by the conjugate flow limit, in which case waves become long and horizontally uniform in the centre. The maximum horizontal velocity in the limiting wave is much less than the wave's propagation speed and as a consequence, waves with trapped cores are not formed in the presence of the surface mixed layer.

1. Introduction

Large-amplitude solitary internal waves are an important topic of wave research, with a number of studies focusing on waves in stratifications for which the buoyancy frequency varies monotonically (e.g. Brown & Christie 1998; Terez & Knio 1998; Grue *et al.* 2000). In this paper the study of waves in monotonic stratifications is extended by investigating the fate of a single solitary wave as it propagates into shallow water at rest. An idealized two-dimensional, inviscid, nonlinear numerical model is used. One motivation for studying the shoaling behaviour of solitary internal waves is the ubiquitous nature of such waves in the variable-depth, stratified coastal ocean (Ostrovsky & Stepanyants 1989; Huthnance 1989). While the monotonic stratifications considered here are not generally found in the ocean, it is hoped that the present study makes a useful contribution to our understanding of the shoaling behaviour of solitary internal waves. This work complements previous laboratory and numerical studies which have focused on two-layer stratifications.

The investigation by the author of shoaling waves for a variety of stratifications has shown that only for nearly monotonic stratifications will waves with trapped cores be formed. Hence, stratifications which increase monotonically in strength towards the surface are considered almost exclusively in this paper. For these stratifications, large waves at the breaking limit, where the maximum horizontal velocity and wave propagation speed are identical, exist. Shoaling waves which break form unsteady, solitary-like waves with trapped cores in the shallow water. The possible existence of waves with trapped cores is of great interest because they would provide a very effective transport mechanism. The effects of modifying the near-surface stratification

by adding a thin surface mixed layer is also briefly considered. It is found that the presence of a thin surface mixed layer greatly inhibits the formation of waves with trapped cores. For the mixed-layer stratification large waves do not reach the breaking limit. Instead, they broaden and become flat in the centre. Such waves are said to be limited by the conjugate flow limit (Benjamin 1966; Lamb & Wan 1998). It is conjectured that waves with trapped cores cannot be formed if the solitary wave amplitudes are limited in amplitude by the conjugate flow limit. This implies that waves with trapped cores would occur rarely in the ocean. Even in places where the stratification allows waves with trapped cores to be formed, the detection of them may be difficult because of the need to make measurements close to the surface of sufficient accuracy to show that fluid velocities are equal to or larger than wave propagation speeds.

While no observations of waves with a trapped core have been made in the ocean, observations of atmospheric solitary waves with trapped cores have been made. In these observations, the fluid in the core is denser than the surrounding fluid, indicative of their association with gravity currents generated by downdraughts from thunderstorms (e.g. Doviak & Christie 1989), cold fronts, or from sea breezes. A spectacular example of the latter is the Morning Glory in northern Australia (Clarke, Smith & Reid 1981; Christie 1992). Atmospheric solitary waves with recirculating cores have also been observed in the nocturnal boundary layer under quiescent conditions (Cheung & Little 1990), but here again the fluid in the core was denser than that in the surrounding air. Waves with trapped cores formed by overturning shoaling waves have core densities equal to that of some of the surrounding fluid. Thus, atmospheric waves have different properties and different generation mechanisms than those considered here.

The experimental analogue of thunderstorm downdraught-generated solitary waves with trapped cores has been conducted by Manasseh, Ching & Fernando (1998). Mode-one waves with trapped cores have been the subject of both theoretical (Derzho & Grimshaw 1997) and laboratory (Grue *et al.* 2000) investigations. Much more experimental work has been done on mode-two waves with trapped cores (Davis & Acrivos 1967; Kamachi & Honji 1982; Stamp & Jacka 1996; Schmidt & Spigel 2000).

As a wave shoals it adjusts to its new environment by changing shape and in so doing may break up into a number of waves. Theoretical studies of shoaling surface and internal solitary waves, based on extensions of the KdV equation, give two useful pictures of the shoaling process (Kakutani 1971; Johnson 1973; Djordjevic & Redekopp 1978; Grimshaw 1983). Adiabatic theory is used when the depth changes slowly compared to the length scale of the wave. It predicts, to a first approximation, that the solitary wave adjusts so that it always has the shape of a solitary wave appropriate to the local water depth. Conservation of wave action flux leads to the prediction that the amplitude of a shoaling surface solitary wave is inversely proportional to the water depth (Boussinesq 1872; Grimshaw 1970). The situation for internal waves is more complicated due to changes in the form of the stratification. A simple amplitude dependence on the local depth is no longer possible (Grimshaw 1983; Holloway *et al.* 1997). Mass is not conserved in adiabatic theory. Higher-order corrections for adiabatically shoaling surface solitary waves predict the appearance of a long shelf behind the solitary wave and a long reflected wave (see Johnson 1994 and references therein). With these modifications mass is conserved.

If the depth changes very quickly, a shoaling wave reaches shallow water before it has time to adjust to the new depth. Theoretical models for rapidly shoaling waves predict that as the wave shoals, the wave form is scaled by a depth-dependent factor.

As a consequence, when it reaches shallow water the wave is no longer a solitary wave and it subsequently breaks up, or fissions, into a number of solitary waves followed by a dispersive wave train. For surface waves, the scaled wave form is proportional to $h^{-1/4}$ where h is the local depth (Johnson 1973). This is merely Green's law for shoaling, long linear waves (Green 1837). The scaling factor is more complicated for internal waves (Djordjevic & Redekopp 1978). When the shoaling wave encounters abrupt depth changes a reflected wave is also created. The shoaling process for internal solitary waves is more complicated than that for surface waves because of the possibility of critical reflection off the bottom and because waves of other modes and vertically propagating waves may be formed.

A number of laboratory investigations on shoaling solitary internal waves have been performed. These have focused exclusively on two-layer fluids using layers of fresh and salty water with a thin interface. The situation where a shoaling solitary wave of depression passes through a turning point was investigated by Helfrich & Melville (1986). Helfrich (1992) considered the case where the interface intercepted the slope. Wallace & Wilkinson (1988) investigated shoaling periodic waves for the same situation. Kao, Pan & Renouard (1985) investigated shoaling solitary waves for the situation where the lower layer depth was greater than the upper layer depth in both deep and shallow water. In this case the shoaling wave does not encounter a turning point. Laboratory studies of shoaling periodic wave trains using linearly stratified water have also been undertaken (Cacchione & Wunsch 1974; Ivey & Nokes 1989). The only numerical simulations of shoaling solitary waves that have been done are those by Saffarinia & Kao (1996) who considered waves passing through a turning point. These authors used a continuous two-layer stratification with a thin pycnocline.

The plan of the paper is as follows. In § 2 the numerical model and the model stratifications are described. In § 3 the method used to compute the initial solitary wave is presented. A general discussion of large-amplitude solitary waves, with a focus on limiting amplitudes for waves with open streamlines, is included here as an aid in interpreting the behaviour of shoaling waves. In § 4 properties of solitary waves for the model stratifications are discussed. Results of the numerical simulations of shoaling waves are given in § 5. In § 6 wave energetics is briefly discussed. A summary and conclusions are given in § 7.

2. The numerical model

The numerical model used in this study is a modified version of the one described in Lamb (1994). Rotation is not included for these simulations. For the most part, the model equations are the incompressible Euler equations with the Boussinesq approximation, namely

$$\boldsymbol{U}_t + \boldsymbol{U} \cdot \nabla \boldsymbol{U} = -\nabla p - \rho g \hat{\boldsymbol{k}}, \tag{1a}$$

$$\rho_t + \boldsymbol{U} \cdot \nabla \rho = 0, \tag{1b}$$

$$\nabla \cdot \boldsymbol{U} = 0, \tag{1c}$$

where standard terminology has been used. The rigid lid approximation is made which removes surface waves from the problem. For the consideration of wave energetics it has been found necessary to damp some numerical instabilities which arose in the deep water behind the incident wave. This is discussed in § 6. The model equations are solved using a second-order projection method (Bell, Colella & Glaz 1989; Bell & Marcus 1992). Terrain-following (sigma) coordinates are used. All model runs use

evenly spaced grid points in the horizontal with a grid spacing δx. There are J grid points in the vertical. In the shallow water a variable vertical grid spacing δz has been used, with δz decreasing quadratically towards the surface in the shallow water. This provides higher resolution in regions where wave breaking occurs. In the deep-water region where the initial wave is added δz is vertically uniform. Unless otherwise stated $\delta x = 2\,\mathrm{m}$ and $J = 120$. In the shallow water the vertical resolution is about 0.53 m at the bottom and 0.14 m at the surface. Some runs used higher vertical resolution ($J = 150$). In addition, some lower resolution runs ($\delta x = 4\,\mathrm{m}$, $J = 100$) were done to verify the accuracy of the results. The initial waves are at $x = -3000\,\mathrm{m}$.

The behaviour of shoaling solitary waves will be explored in greatest depth using exponential stratifications of the form

$$\bar{\rho}_1(z) = 1 + 0.01\frac{1 - \mathrm{e}^{(z-H)/S}}{1 - \mathrm{e}^{-H/S}}. \tag{2}$$

Here, the surface is at $z = H$ where $H = 100\,\mathrm{m}$ is the deep water depth. Results using three different scale heights, $S = 15$, 35 and 75 m, will be presented. A hyperbolic tangent density profile of the form

$$\bar{\rho}_2(z) = 1 - 0.01\frac{\tanh(z - H/S)}{\tanh(H/S)} \tag{3}$$

is also considered, using scale heights $S = 20$ and 45 m. These values of S yield similar density profiles to the exponential densities with $S = 15$ and 35 m. Both these density profiles have a non-dimensional surface to bottom density change of 0.01 in the deep water. They also have the property that the buoyancy frequency $N(z)$ is a monotonically increasing function of z. For the exponential stratifications $N'(z)$ is an increasing function of z whereas for the hyperbolic tangent density $N'(z)$ takes its maximum value a distance $0.88S$ below the surface and is zero at the surface. For waves in a fluid of depth D, the ratio S/D determines the properties of the solitary waves so changing S is equivalent to changing the shallow water depth. To obtain precisely the same change in shoaling behaviour by changing the shallow water depth as by changing the scale height one would need to change the deep water depth and the shelf width appropriately. Properties of solitary waves for both these stratifications have been considered by Brown & Christie (1998).

To demonstrate the sensivity of the results to the near-surface stratification, a third stratification is also briefly considered. This stratification is obtained by modifying (2) with $S = 15\,\mathrm{m}$ to include an upper mixed layer approximately 2 m thick. This modified density is given by

$$\bar{\rho}_{m1}(z) = 1 + 0.01\frac{1 - \mathrm{e}^{(z-H)/15}}{1 - \mathrm{e}^{-H/15}}\left(1 - \tanh\left(\frac{z - H + 3.0}{2}\right)\right) + 0.0005\,(1 - 0.02(z - H))\left(1 + \tanh\left(\frac{z - H + 3.0}{2}\right)\right). \tag{4}$$

The stratifications used in this study are shown in figure 1. The exponential stratification with scaleheight $S = 15\,\mathrm{m}$ has a relatively large change in N over the water column in the shallow water. For $S = 75\,\mathrm{m}$ the variation is considerably reduced with N increasing approximately linearly toward the surface. For large S/H, N becomes nearly constant, which is the type of stratification considered by Derzho & Grimshaw (1997).

The evolution of the wave as it shoals will depend on the form of the topography.

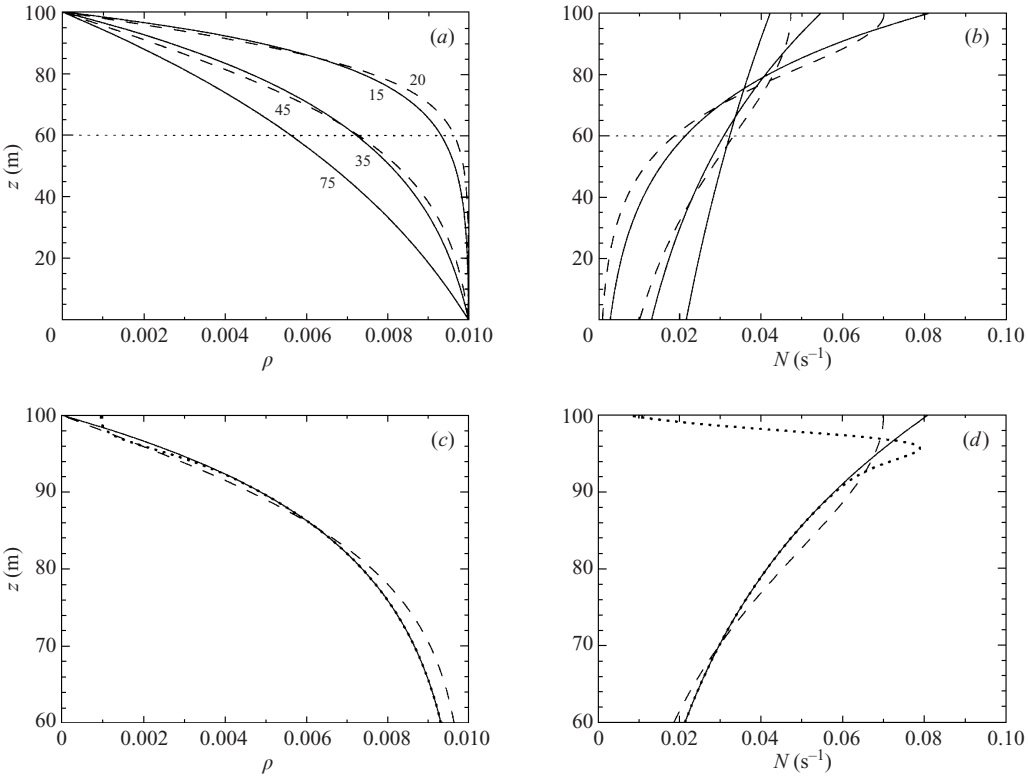

FIGURE 1. Density and buoyancy frequency profiles for model stratifications. (*a*) Exponential densities $\bar{\rho}_1(z)$ for scale heights $S = 15$, 35 and 75 m (solid) and hyperbolic tangent density $\bar{\rho}_2(z)$ for $S = 20$ and 45 m (dashed). Horizontal dotted line indicates height of shelf. (*b*) Buoyancy frequency profiles for stratifications shown in (*a*). (*c*) Comparison of $\bar{\rho}_1(z)$ for $S = 15$ m (solid), $\bar{\rho}_2(z)$ (dashed) and the mixed-layer stratification $\bar{\rho}_{m1}$ (dotted). Upper 40 m only. (*d*) Buoyancy frequency profiles for stratifications shown in (*c*).

For simplicity we restrict attention to a single shelf slope given by a hyperbolic tangent profile. Thus, the bottom is at

$$z = h(x) = \frac{a_T}{2}\left(1 + \tanh\left(\frac{x}{L}\right)\right). \tag{5}$$

The amplitude a_T is fixed at 60 m, so that the waves shoal from a depth of 100 m to a depth of 40 m in all cases. Three shelf widths, $L = 200$, 400 and 600 m, are considered.

The shallow-water environment determines the properties of the waves in shallow water, hence the shallow water depth $D = H - a_T$ is the natural length scale of the problem. For model runs using densities $\bar{\rho}_1$ and $\bar{\rho}_2$ there are three non-dimensional parameters: a_T/D, S/D and L/D. For fixed values of these parameters, all distances scale with D. In particular, the values of these parameters determine whether or not waves with trapped cores are formed, the amplitudes of the shoaled waves, the breaking depth, etc. An appropriate velocity scale in the shallow water is $\sqrt{\Delta\rho g D}$ where $\Delta\rho$ is the bottom to surface density difference in the shallow water. For the inviscid calculations presented here the velocity scale is not qualitatively significant, it merely affects the time at which events occur. An important non-dimensional number for solitary waves is the ratio of the propagation speed to the maximum horizontal velocity in the wave $c/U_{\max}$. This ratio is independent of $\Delta\rho$.

3. Solitary wave initialization and limiting wave amplitudes

The initial solitary waves are computed using a reference frame in which the wave is stationary. The equations of motion (1) then yield the nonlinear solitary wave eigenvalue problem

$$\nabla^2\eta + \frac{N^2(z-\eta)}{c^2}\eta = 0, \tag{6}$$

with boundary conditions $\eta = 0$ at $z = 0, H$ and $\eta \to 0$ as $x \to \pm\infty$. Here $\eta(x,z)$ is the vertical displacement of the streamline passing through (x,z) relative to its far-field height, the eigenvalue c is the wave propagation speed and

$$N^2(z) = -g\frac{\mathrm{d}\bar{\rho}}{\mathrm{d}z}(z) \tag{7}$$

is the square of the buoyancy frequency outside the wave where $\bar{\rho}(z)$ is the undisturbed density field non-dimensionalized by the fixed reference density. Equation (6) is the Dubreil–Jacotin–Long (DJL) equation written in terms of the streamline displacement, which, for the special case considered here (no background current), is proportional to the perturbation stream function. It is solved using a variational technique to minimize the kinetic energy for a specified value, A, of the functional

$$F(\eta) = \frac{1}{H}\iint_R \int_0^{\eta(x,z)} (\bar{\rho}\,(z-\eta(x,z)) - \bar{\rho}\,(z-s))\,\mathrm{d}s\,\mathrm{d}x\,\mathrm{d}z, \tag{8}$$

where R is the computational subdomain in which the initial wave is computed (Turkington, Eydeland & Wang 1991). The available potential energy of the wave in an infinitely long domain is equal to $gHF(\eta)$. Wave amplitudes are specified by a choice of a value for A, hence the maximum vertical displacement of an isopycnal is not chosen *a priori*. Other authors have used different techniques to solve the DJL equation (Davis & Acrivos 1967; Tung, Chan & Kubota 1982; Brown & Christie 1998). Only mode-one solitary waves can be computed since the derivation of the DJL equation assumes a wave of permanent form. Higher-mode solitary-like waves are accompanied by trailing, lower-mode, dispersive waves which imply a continual energy loss from the solitary-like wave and hence non-steadiness (Akylas & Grimshaw 1992). Once η and c are known the density and velocity fields are given by

$$\rho(x,z) = \bar{\rho}(z-\eta(x,z)), \tag{9a}$$

$$(u,w) = (c\eta_z, -c\eta_x). \tag{9b}$$

The solitary waves with open streamlines that can be calculated are limited in amplitude in three ways.† For small waves, in a reference frame fixed with the fluid at infinity, the wave propagation speed c is close to the linear long-wave propagation speed and the maximum horizontal fluid velocity in the direction of wave propagation, $U_{\max}$, is much smaller than c. As the wave amplitude increases $U_{\max}$ increases more rapidly than c. For some stratifications a wave amplitude is reached at which $U_{\max} = c$. This point is reached when a streamline, in a reference frame moving with the wave, first becomes vertical. This limiting amplitude will be called the breaking limit. Larger waves, with closed streamlines in a recirculating wave core, can be computed. They are convectively unstable because for these waves $z - \eta$ goes above/below the fluid domain for waves of depression/elevation and the density in the centre of the core is

† The terminology open and closed streamlines will always be used in a reference frame moving with the wave.

lighter/denser than the surrounding fluid. This occurs because only for stratifications with non-zero density gradients at the upper/lower boundary has the breaking limit been reached. A few attempts to compute large waves with N^2 decreasing to zero rapidly at the upper/lower boundary have been made. They were unsuccessful due to failure of the numerical scheme to converge (see discussion of the stability limit below). The solution method also does not converge when there are discontinuities in N at the upper boundary. This may be a problem with the numerical method and not a fundamental limitation. In monotonic stratifications (N increases or decreases monotonically) wave amplitudes are limited by either the breaking limit or by the stability limit discussed below.

Wave amplitudes can also be limited by the conjugate flow limit (Benjamin 1966; Lamb & Wan 1998). In this situation large waves become flat in the centre and simply become longer as the energy in the wave increases. Wave properties such as the maximum isopycnal displacement $\eta_{\max}$ (taken positive for waves of depression and elevation), c and $U_{\max}$ asymptotically approach constant limiting values as the waves flatten in the centre. This limiting behaviour is typical of stratifications with broad pycnoclines well removed from the upper or lower boundaries. The horizontally uniform flow in the centre of long flat waves is called a conjugate flow and can be found by solving the nonlinear conjugate flow eigenvalue problem

$$\left.\begin{aligned} \eta''(z) + \frac{N^2(z-\eta(z))}{c^2}\eta(z) = 0, \\ \eta(0) = \eta(H) = 0, \end{aligned}\right\} \tag{10}$$

along with an auxiliary condition,

$$\int_0^H \eta'^3(z)\,\mathrm{d}z = 0, \tag{11}$$

which is determined from conservation of momentum flux (Benjamin 1966; Lamb & Wan 1998). In addition, a conjugate flow solution must satisfy the condition that $\eta'(z) < 1$ in order that all streamlines extend to $\pm\infty$. Note that (10) can be obtained from (6) by taking η to be independent of x. Lamb & Wan (1998) showed that monotonic stratifications do not have mode-one conjugate flow solutions.

The third way in which wave amplitudes can be limited is by what will be called the stability limit. As solitary wave amplitudes increase, the minimum Richardson number in the stratified region of fluid, Ri_m, decreases. For some stratifications the iteration procedure used to solve (6) fails to converge before either the breaking limit or the conjugate flow limit is reached. This typically occurs when Ri_m is close to 0.25 (waves with minimum Richardson numbers as low as 0.23 have been computed). As is well known, a minimum Richardson number of less than 0.25 in the flow interior is necessary for a parallel stratified flow to be unstable (Miles 1961; Howard 1961). This criterion is widely used to predict instability of internal waves, although Hazel (1972) has reported on a parallel stratified flow which is stable for minimum Richardson numbers above about 0.2. Since flow in a solitary wave is not parallel, the Richardson number criterion for predicting instability of a solitary wave should be used with caution. The convergence failure of the iteration procedure for Richardson numbers close to 0.25 suggests that it is because waves are close to being physically unstable, hence we call this amplitude limitation the stability limit. This limit is typically reached for stratifications with thin pycnoclines centred away from the mid-depth. An extreme example of this is a two-layered fluid. It is well known that large solitary

waves become flat-centred (Turner & Vanden-Broeck 1988). The two-layer conjugate flow in the centre of these waves is unstable due to a velocity jump across the interface.

The one-dimensional conjugate flow equations (10) and (11) are not subject to the same stability limitations as is the solitary wave eigenvalue problem (6). Hence, conjugate flows with arbitrarily low minimum Richardson numbers, which could be two-dimensionally unstable, can be computed.

Interestingly, the numerical procedure used to solve the DJL equation to obtain the initial solitary waves can yield convectively unstable solitary waves with closed streamlines, yet waves with a shear instability can apparently not be computed. This may be due to the different sources of energy for the instability (potential and kinetic respectively) and the fact that the solution procedure is based on a variational formulation which minimizes the kinetic energy for a specified available potential energy. Other solution methods of the DJL equation can also result in convectively unstable waves with trapped cores (Tung *et al.* 1982; Brown & Christie 1998).

Waves with amplitudes beyond the wave breaking limit have been investigated by other authors. Mode-two solitary-like waves with recirculating cores have been observed experimentally (Davis & Acrivos 1967; Kamachi & Honji 1982; Stamp & Jacka 1996). Recently Grue *et al.* (2000) have generated mode-one solitary waves with recirculating cores in the laboratory. They used a continuously stratified fluid composed of a layer of constant N overlying or underlying a layer of constant density (a monotonic stratification). Solitary mode-one internal waves with recirculating cores have also been computed numerically; however, there is uncertainty regarding the correct properties of the fluid inside the recirculating region (Tung *et al.* 1982; Brown & Christie 1998). Assuming a constant density in the core, Derzho & Grimshaw (1997) have predicted that to leading order the fluid inside the core should be stagnant, i.e. non-circulating, in a reference frame moving with the wave. They considered stratifications for which the buoyancy frequency is nearly uniform yielding a finite-amplitude weakly nonlinear theory (at leading order the equations are linear due to the nearly constant N). Because of this, waves with closed streamlines will generally be referred to as having trapped cores, although in all results presented herein the core is recirculating. It is unclear whether stable waves of permanent form having trapped cores exist.

Some of the time-dependent numerical simulations of unsteady large-amplitude solitary internal waves on a thin interface by Terez & Knio (1998) include mode-one waves with recirculating cores. They considered waves on a thin pycnocline centred at the mid-depth and, assuming symmetry across the mid-depth, restricted their computational domain to the upper half of the domain. Thus, while claiming to study mode-two waves, they in fact computed mode-one solitary waves in a fluid with a thin stratified layer adjacent to a lower boundary. The buoyancy frequency N decreased monotonically with height above the boundary. For such a stratification waves with open streamlines are limited in amplitude by the breaking limit.

4. Properties of solitary waves

Solitary mode-one waves are waves of depression in both the deep and shallow water for all stratifications considered. Hence, no turning point is encountered as the waves shoal. For stratifications $\bar{\rho}_1$ and $\bar{\rho}_2$ wave amplitudes are limited by the breaking amplitude in all depths. For the mixed-layer stratification $\bar{\rho}_{m1}$, wave amplitudes are bounded by the stability limit in deep water and by the conjugate flow limit in shallow water. Solitary waves close to breaking have their maximum velocity at the surface.

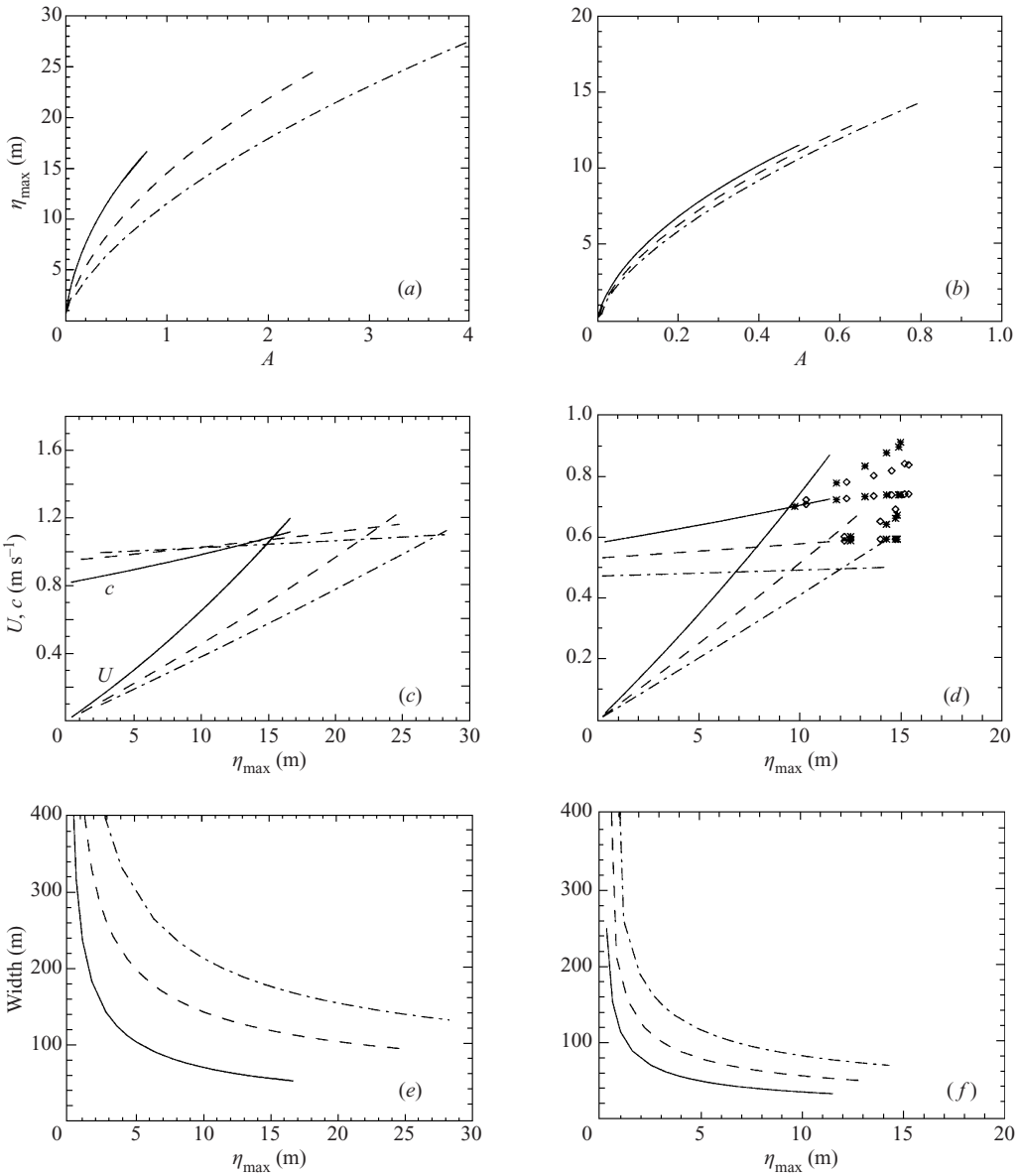

FIGURE 2. Solitary wave properties for exponential stratifications using $S = 15$ m (solid), 35 m (dashed) and 75 m (dash-dot): (a, c, e) deep water (100 m depth); (b, d, f) shallow water (40 m depth). Plotted in (a, b) are wave amplitudes as a function of A, the value of the potential energy functional $F(\eta)$. (c, d) The propagation speed c and maximum horizontal velocity U_{max} and (e, f) the wave half-width plotted as functions of solitary wave amplitudes. In addition, the propagation speed and maximum horizontal velocity for waves with trapped cores obtained from model runs using $S = 15$ and 35 m are shown in (d). Stars are results obtained using a shelf width of 200 m, diamonds for a shelf width of 600 m. For these waves U_{max} is larger than c.

Assuming that $U_{max} = c$ first occurs at the surface, it is easily seen from (6), (9*a*) and (9*b*) that the horizontal shear u_z and the vertical density gradient are zero at the point where $U_{max} = c$. The minimum Richardson number stays well above 0.25 as the breaking amplitude is approached for stratifications (2) and (3), although it can be

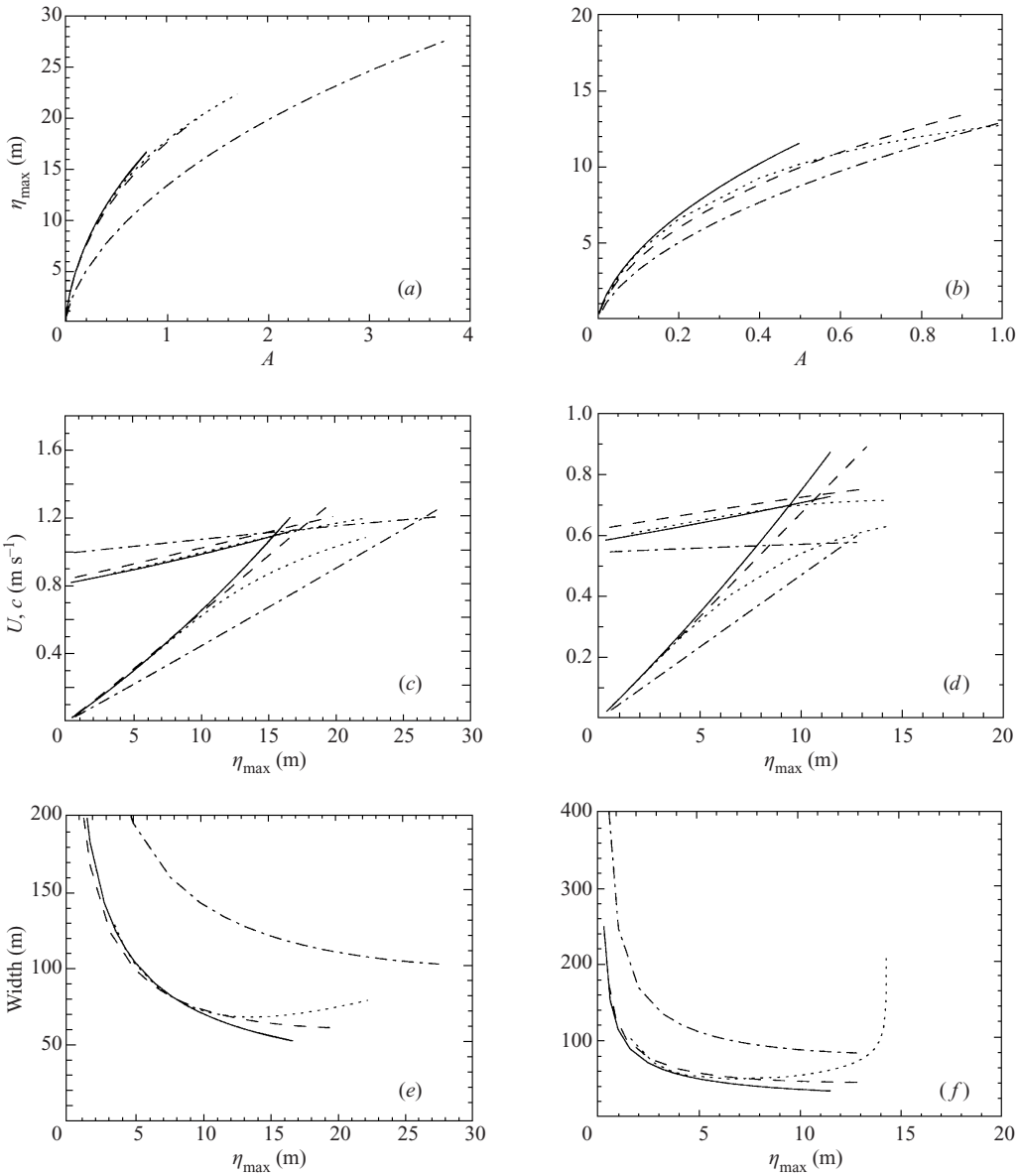

FIGURE 3. As in figure 2 but for exponential stratification with $S = 15$ m (solid), hyperbolic tangent density with $S = 20$ (dashed) and $S = 45$ m (dash-dot) and for the mixed-layer stratification (dots).

below 0.25 for other stratifications. For example, for the exponential stratification Ri_m is approximately 0.6 at the breaking amplitude in both the deep and shallow water for scale heights of 15 and 75 m. For stratifications with nearly constant N, Clarke & Grimshaw (1999) have shown that the Ri_m is $O(1)$.

In figures 2 and 3 the wave amplitude, $\eta_{max} = \max|\eta|$, is plotted as a function of A, the value of the functional $F(\eta)$ used to specify wave amplitudes in the solitary wave solver. Also shown are the wave propagation speed c, the maximum horizontal velocity U_{max}, and half-width plotted as functions of η_{max}. Values in water depths of 100 and 40 m are presented. Figure 2 shows the results for the three exponential

stratifications. It includes some values for the physically unrealizeable, convectively unstable waves beyond the breaking limit where $U_{\max} > c$. The breaking amplitudes increase with S, being approximately 15.5, 23.3 and 27.7 m for scale heights of 15, 35 and 75 m respectively. At the breaking amplitude the propagation speeds are approximately 1.09, 1.15 and 1.09 m s^{-1} respectively. In a depth of 40 m, because of the reduction in the surface to bottom density change associated with an increase in S, both c and $U_{\max}$ are decreasing functions of S for all wave amplitudes. The breaking amplitudes increase with S, being 9.5, 11.4 and 12.1 m. This trend, as expected, is the same in both water depths since the ratio $U_{\max}/c$, and hence the breaking amplitude, depends only on the shape of the density profile and is independent of the surface to bottom density change. Propagation speeds at the breaking amplitude in shallow water decrease with S, being 0.70, 0.58 and 0.49 m s^{-1}. The wave half-width is defined as the distance from the centre of the wave at which the surface velocity is equal to half the surface velocity at the wave centre. The half-width is a decreasing function of $\eta_{\max}$ and an increasing function of S. Wave widths are smaller in the shallow water than in the deep water for a given wave amplitude.

In figure 3 the wave properties for the hyperbolic tangent density $\bar{\rho}_2$ with $S = 20$ and 45 m and for the mixed-layer density $\bar{\rho}_{m1}$ are compared with those for the exponential stratification $\bar{\rho}_1$ using $S = 15$ m. Wave properties for stratifications $\bar{\rho}_1$ with $S = 15$ m and $\bar{\rho}_2$ with $S = 20$ m are similar, with the latter having larger breaking amplitudes. This is associated with a slight increase in propagation speeds for all wave amplitudes and with a decrease in $U_{\max}$ for large-amplitude waves. Note $U_{\max}$ is very similar for small waves. For a specified wave amplitude, larger values of A are required for density $\bar{\rho}_2$. The effects of increasing S in densities $\bar{\rho}_1$ and $\bar{\rho}_2$ are qualitatively identical.

Comparing the properties of waves for the exponential and mixed layer stratifications shows that maximum wave currents in large solitary waves are sensitive to changes in the near-surface density. A small change in the density can result in a large change in the buoyancy frequency and it is the latter which is dynamically important. Reducing N near the surface reduces the baroclinic generation of vorticity and hence the vertical shear of the horizontal velocity near the surface above the wave. Strengthening this effect is the fact that the layer of modified density near the surface is stretched vertically when it passes over the centre of the wave and becomes much thicker than 2 m. For large waves the result is a thick layer of reduced N and of reduced vorticity. This is responsible for the large decrease in $U_{\max}$. It also partially accounts for the reduction of $U_{\max}$ in large waves for density $\bar{\rho}_2$ compared to those for density $\bar{\rho}_1$ and for the decrease in $U_{\max}$ as S increases for either of these stratifications, although the effect is not as pronounced. In figure 4 the vertical profiles of the horizontal velocity down the centre of two solitary waves, one each for the exponential ($S = 15$ m) and mixed-layer stratifications, are compared. The waves have the same value of A and have different amplitudes (14.3 and 14.0 m respectively). The velocity profiles are similar in the lower 90 m. For the mixed-layer stratification u is almost constant in the upper 8 m.

Because the vertical stretching is greatest at the surface(bottom) for waves of depression(elevation), one can expect that mode-one solitary waves of depression(elevation) will be most sensitive to changes in stratification near the upper(lower) boundary.

The mixed-layer density $\bar{\rho}_{m1}(z)$ has a conjugate flow which can easily be found by solving (10)–(11). In 100 m depth the isopycnal which undergoes the maximum downward displacement in the conjugate flow is initially about 5.7 m below

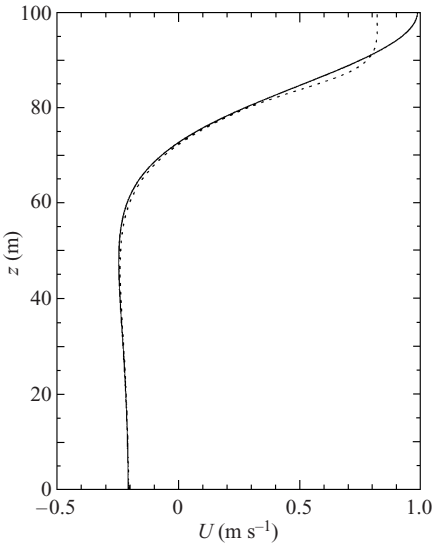

FIGURE 4. Vertical profiles of the horizontal velocity down the centre of two solitary waves in water of depth 100 m. One wave is in the exponential stratification with $S = 15$ m (solid). The other wave is in the mixed-layer stratification (dotted). Wave amplitudes are 14.3 and 14.0 m respectively.

the surface and is displaced down by 43.7 m to close to the mid-depth. In comparison, for the undisturbed stratification, the buoyancy frequency maximum is approximately 4.3 m below the surface. The conjugate flow has a propagation speed of $1.322\,\mathrm{m\,s^{-1}}$, bottom and surface currents of -1.324 and $1.306\,\mathrm{m\,s^{-1}}$ respectively, and a minimum Richardson number of 0.10. The latter suggests that the conjugate flow is unstable and therefore that stable flat-centred waves do not exist. Only solitary waves with an amplitude below 22 m, about half the amplitude of the conjugate flow, can be calculated with the numerical method used to solve (6). The maximum horizontal current in the direction of wave propagation, $U_{\max}$, is below the surface for amplitudes larger than about 5 m. The location of the maximum current gradually moves deeper as the waves get larger and is about 4 m below the surface for the 22 m wave. The difference between the maximum current and the maximum surface current is, however, extremely small, the maximum difference being about $0.0004\,\mathrm{m\,s^{-1}}$ for a 16 m wave (compared with $U_{\max} = 0.9020\,\mathrm{m\,s^{-1}}$).

As the water depth decreases, the maximum isopycnal displacement for the conjugate flow decreases, as do the bottom and surface currents, and Ri_m increases. In a depth of 40 m solitary waves are limited in amplitude by the conjugate flow limit. The conjugate flow has an amplitude of 14.3 m with the isopycnal undergoing this maximum downward displacement having a rest height 5.3 m below the surface. The minimum value of the Richardson number in the conjugate flow is 0.285 and this occurs 2.5 m above the isopycnal undergoing the maximum displacement. The conjugate flow propagation speed is $0.710\,\mathrm{m\,s^{-1}}$, while the bottom and surface currents are -0.653 and $0.624\,\mathrm{m\,s^{-1}}$ respectively. These values provide limiting maximum values for solitary internal waves in water of 40 m depth for the mixed-layer density $\bar{\rho}_{m1}$. The bottom current is larger in magnitude than the surface current in both water depths. Large solitary waves have this property as well.

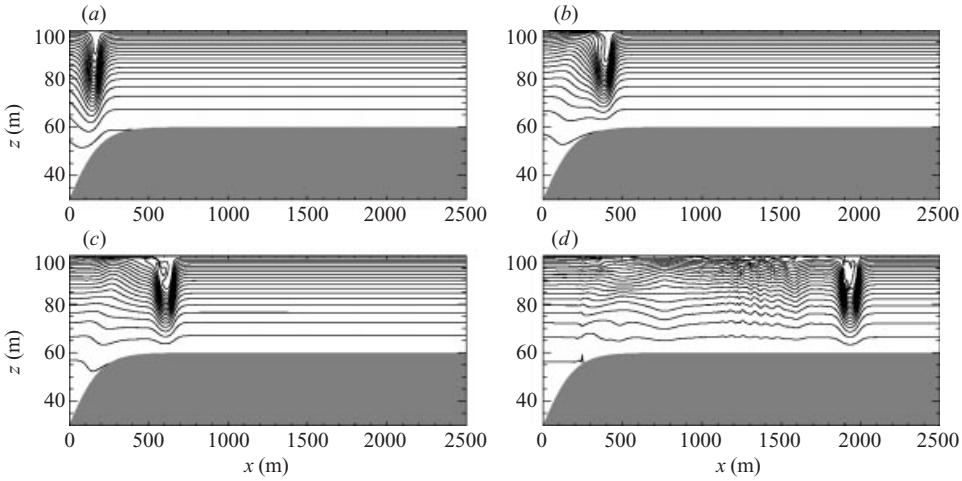

FIGURE 5. Density contour plots using exponential stratification with $S = 15$ m. Shelf width is $L = 200$ m and initial wave amplitude is 14.3 m. (*a*) $t = 50$ min, (*b*) $t = 55$ min, (*c*) $t = 60$ min, (*d*) $t = 90$ min.

5. Evolution of shoaling waves

We now consider the shoaling characteristics of waves. In all cases, as waves shoal they increase in amplitude over the shelf slope and steepen at the back, as reported by Kao *et al.* (1985) and Saffarinia & Kao (1996). If the initial wave is sufficiently large, the back of the wave may overturn and wave breaking commences. No evidence of a shear instability, as reported by Kao *et al.* (1985), has been detected here. Their two-layer stratification, however, is quite different from the stratifications used in this study. On the shelf a leading solitary-like wave emerges which gradually changes shape as it adjusts to its new depth. Trailing it may be other, smaller, solitary-like waves, a mode-one dispersive wave train, a large mode-two solitary-like wave and other higher-mode waves. Reflected waves are also generated, although they are usually too small to detect in density contour plots. For large initial waves breaking occurs over the shelf slope; however for smaller waves using the monotonic stratifications $\bar{\rho}_1$ or $\bar{\rho}_2$ wave breaking may occur well onto the shelf. This is a result of the fact that, for these stratifications, the leading wave grows in amplitude as it adjusts to its new environment. For both of these stratifications wave breaking results in the formation of waves with trapped cores. For the mixed-layer stratification wave breaking only occurs over the shelf slope and is short lived. Waves with trapped cores are not formed.

We begin by illustrating a variety of shoaling behaviours by presenting density contour plots from a number of cases.

As an example of a breaking wave which forms a trapped core consider the case of an initial wave of amplitude 14.3 m ($A = 0.6$) using the exponential stratification with $S = 15$ m and a shelf-slope width $L = 200$ m. Contour plots of the density field are shown at four different times in figure 5. As the wave shoals it steepens at the back and first overturns near the top of the slope at $x = 251$ m in a depth of 44.5 m. Fluid from near the surface then plunges forward, filling the depression ahead of it. This fluid forms the core of the resulting non-steady solitary-like wave and is slightly denser than both the fluid at the surface and the fluid just below the core. The density in the centre of the core is equal to that of the undisturbed density

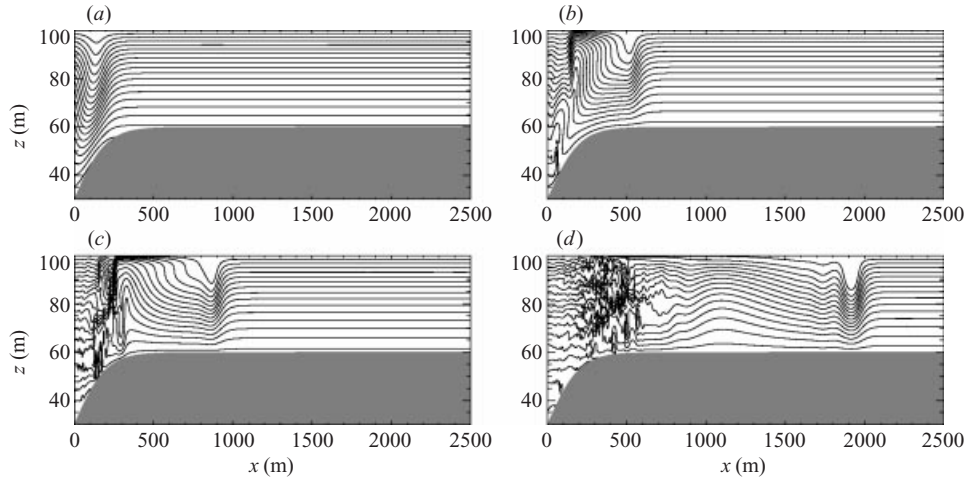

FIGURE 6. As in figure 5 but with density scale height $S = 35$ m. Initial wave amplitude 14.5 m. (*a*) $t = 50$ min, (*b*) $t = 60$ min, (*c*) $t = 70$ min, (*d*) $t = 100$ min.

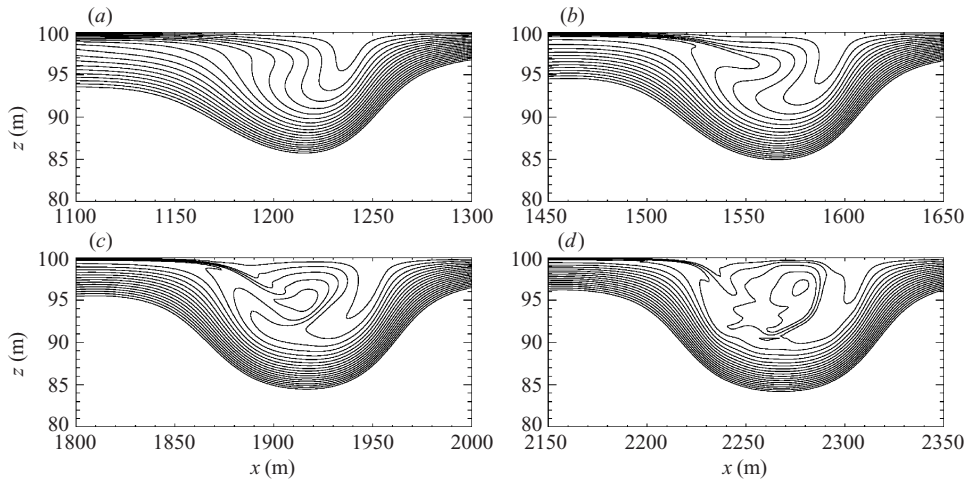

FIGURE 7. Close-up look at the formation of wave with trapped core. Same case as shown in figure 6. (*a*) $t = 80$ min, (*b*) $t = 90$ min, (*c*) $t = 100$ min, (*d*) $t = 110$ min.

about 2 m below the surface. The density of the fluid in the core decreases with time as the wave evolves, due to mixing and numerical diffusion. By $t = 90$ min, the wave field has separated into several distinct features. Farthest on the shelf is the large solitary wave with the trapped core. Trailing it is a second solitary wave of much smaller amplitude and then a mode-one dispersive wave train of small amplitude (at $x \approx 1600$ and 1100–1500 m respectively). Behind the wave train is a long mode-two wave ($x \approx 900$ m). The wave field over the top of the slope is more complex.

Results from a model run using the exponential stratification with $S = 35$ m are presented in figures 6 and 7. The initial wave amplitude is 14.5 m ($A = 1.0$) and the shelf-slope width is 200 m. At $t = 50$ min the wave is nearing the top of the shelf-slope in water with a depth of approximately 50 m. The wave is tilted, with the bottom of the wave lagging the top of the wave. This occurs for waves using $S = 15$ m as well but is much more pronounced here. Vigorous overturning commences at the bottom

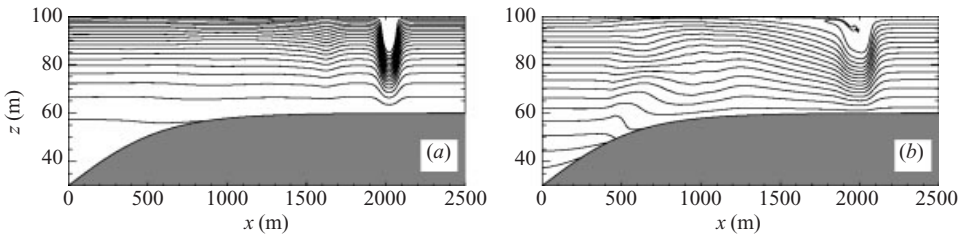

FIGURE 8. Shoaled waves for wider shelf ($L = 600$ m). (*a*) Same density and initial wave as in figure 5 at $t = 90$ min. (*b*) Same density and initial wave as in figure 6 at $t = 100$ min.

($t = 60$ min) and then spreads upward to the right. One possible interpretation of this is as a hydraulic jump associated with the strong off-shelf flow near the bottom under the shoaling wave. Isopycnal displacements behind the lead wave, at $x \approx 100$–300 m, are much larger than in the case using the smaller scale height. The leading wave grows in amplitude as it adjusts to its shallow water environment (figure 6*b*–*d*). Figure 7 shows how it overturns and forms a wave with a trapped core. This occurs well onto the shelf, with wave overturning commencing at $x \approx 1000$ m. The leading wave has a trapped core which forms by $t = 100$ min at which time a large mode-one wave of elevation can be seen propagating ahead of a complex wave field (figure 6). In contrast to cases with $S = 15$ m, for which overturning occurs in two disjoint regions, one near the surface in the overturning lead wave and one at the bottom, for stratifications with $S = 35$ and 75 m overturning can occur in a single broad region which extends from the bottom to the surface along a sloping curve. For the case shown in figure 6, overturning first occurs near the bottom. The region of overturning then spreads upward in the on-shelf direction. A separate patch occurs when overturning in the lead wave takes place as shown in figure 7. For large initial waves, however, overturning first occurs near the bottom and then rapidly progresses upward to the right into the leading wave. There are no longer two disjoint patches of breaking.

In figure 8 results from model runs using the same two stratifications and initial waves but for wider shelf slopes ($L = 600$ m) are shown. The leading solitary waves, which again have a trapped core, are larger and the trailing waves are greatly reduced in amplitude. Very few waves can be detected behind the leading solitary wave. For the case with $S = 35$ m, vigorous overturning did not occur near the bottom in this case, although it does for larger initial waves.

When the mixed-layer stratification is used ($L = 200$) a wave with an initial amplitude of 14.0 m overturns slightly as it shoals but the overturning region quickly disappears (not shown). This is in contrast to the case shown in figure 5 where a wave of similar amplitude forms a wave with a trapped core. The leading solitary wave is close to maximum amplitude.

In figure 9 surface velocity profiles, $u(x, H, t)$, are compared for the 14.0 m wave in the mixed-layer stratification and the 14.3 m wave in the exponential stratification. The initial wave velocities are similar except in the centre of the wave, where the velocities for the exponential stratification are much larger. At $t = 55$ min the two waves are almost in the same position. This is expected since most of their time has been spent in deep water where their propagation speeds are similar (see figure 3). At $t = 55$ min the wave for the exponential stratification has started to overturn (see figure 5) and by $t = 100$ min has formed a trapped core of fluid. This is indicated by the velocity minimum over the centre of the wave. It is now propagating faster than

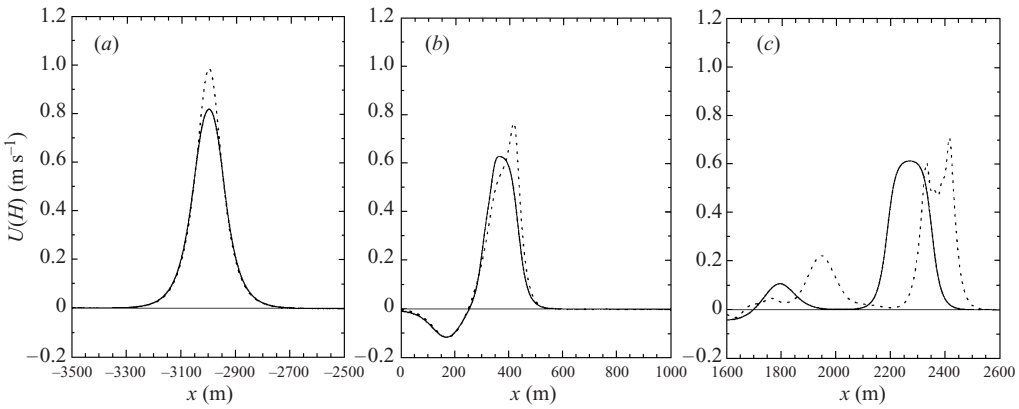

FIGURE 9. Surface velocity profiles for two waves at (*a*) $t = 0$, (*b*) $t = 55$, and (*c*) $t = 100$ min. Solid curves: exponential density with $S = 15$ m, initial amplitude 14.3 m. Dotted curves: mixed layer density, initial amplitude 14.0 m.

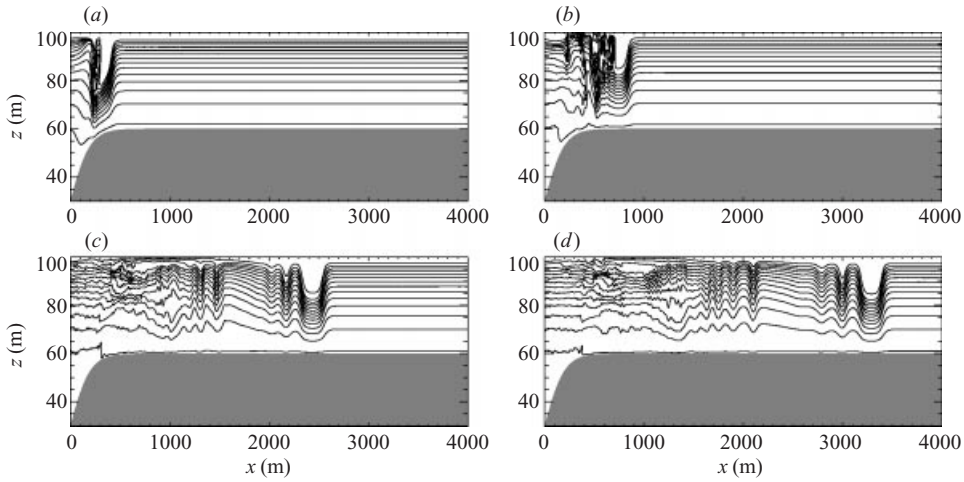

FIGURE 10. Shoaling wave for mixed-layer density. Initial wave amplitude 21.2 m. $L = 200$ m. (*a*) $t = 50$ min, (*b*) $t = 60$ min, (*c*) $t = 100$ min, (*d*) $t = 120$ min.

the wave in the mixed-layer density. The latter wave is now wider and does not have a velocity minimum over the centre of the wave. This is indicative of the fact that it does not have a trapped core. It is close to maximum amplitude as indicated by surface peak velocity of about 0.61 m s^{-1} compared with 0.62 m s^{-1} for the conjugate flow.

Results for a larger wave in the mixed-layer stratification are shown in figure 10. The initial wave amplitude is 21.2 m ($\delta x = 2.0$, $J = 150$). This is close to the maximum initial wave that could be computed. As the wave shoals it steepens at the back until it overturns. At $t = 50$ min the maximum horizontal velocity (1.08 m s^{-1}) occurs in the forward plunging fluid. In comparison, the peak surface velocity is about 0.635 m s^{-1} which is larger than the fluid velocity at the surface in the conjugate flow in 40 m depth (0.624 m s^{-1}), but smaller than the conjugate flow propagation speed (0.710 m s^{-1}). The forward plunging fluid fails to reach the front of the wave and a wave with a core of trapped fluid is not formed. For the case of an exponential

stratification the shoaling wave was much narrower and was filled up by the forward plunging fluid. At $t = 120$ min the leading solitary wave is a flat-centred wave with a width of about 300 m. It has a minimum Richardson number of about 0.285, equal to that for the conjugate flow. The maximum surface velocity is $0.615\,\mathrm{m\,s^{-1}}$, slightly less than the corresponding value of $0.624\,\mathrm{m\,s^{-1}}$ for the conjugate flow (the difference is possibly not numerically significant).

Four model runs were done using larger shallow-water depths to determine what waves were formed when the minimum Richardson number in the shallow-water conjugate flow is less than 0.25. Using $L = 200$ m, shallow-water depths of 60, 55, 50 and 45 m were considered. In these depths the conjugate flow has minimum Richardson numbers of 0.172, 0.190, 0.214, and 0.244 respectively. The initial wave amplitude was the same as that used in figure 10 (21.2 m) in all cases, having a minimum Richardson number of approximately 0.32. As the shallow-water depth increases the overturning becomes less vigorous. For a shallow-water depth of 55 m the shoaling wave overturned slightly for a brief period of time but no significant overturning occurred. No overturning occurred when the shallow-water depth was 60 m. The minimum Richardson number in the leading solitary wave in shallow-water depths of 60, 55, 50, 45 and 40 m was approximately 0.235, 0.237, 0.238, 0.258 and 0.285 respectively. There was no evidence of a shear instability.

5.1. *Evolution of wave amplitudes and velocities*

The evolution of the wave amplitudes, $\eta_{\max}$, the maximum horizontal velocity $U_{\max}$, and the propagation speed c of the leading wave for a large number of cases are shown in figures 11–14 for four stratifications: $\bar{\rho}_1$ for $S = 15$, 35, and 75 m and for the mixed-layer stratification. The propagation speed c is the average over a 300 s interval and is determined from the position where the horizontal velocity at the surface is $0.2\,\mathrm{m\,s^{-1}}$. For the cases shown, the maximum downward isopycnal displacements and maximum horizontal velocities generally occur in the leading solitary wave throughout the model runs. An exception occurs for some of the large wave cases using $S = 35$ and 75 m when the maximum displacement may occur behind the leading wave. For example, for $L = 200$ m and $S = 35$ m at $t = 60$ min the maximum displacement is at $x = 125$ m while the wave is at $x = 500$ m (see figure 6). This only occurs for a brief period of time. In figure 12(*a*) this is the case for model runs for values of x between 0 and 400 m.

For the exponential stratification with scale heights of 15 and 35 m results are presented for shelf-slope widths of $L = 200$ and 600 m (figures 11 and 12). In all cases, the final wave amplitude is larger for the wide than for the narrow shelf slope. This indicates that there is more energy in the leading solitary wave for the wider shelf slopes, as predicted by theory. For the cases with $S = 35$ m there is a limiting wave amplitude of about 14.9 m in the shallow water. For the wide shelf slope, waves with initial amplitudes of 14.5, 17.7 and 20.5 m result in a shoaled solitary wave of this amplitude (figure 12*c*). For the narrower shelf slope the initial wave with amplitude 14.5 m results in a leading shoaled wave with slightly smaller amplitude (figure 12*a*). For a scale height of 15 m there is also a suggestion of a limiting amplitude in the shallow water.

The dashed line in the amplitude plots indicates the shallow-water breaking amplitude. For cases in which the final wave amplitude exceeds the shallow-water breaking amplitude the shoaling waves overturned and formed waves with trapped cores. For cases with final amplitudes below the breaking amplitude, waves with trapped cores were not formed. In these cases wave breaking in the upper half of the fluid column

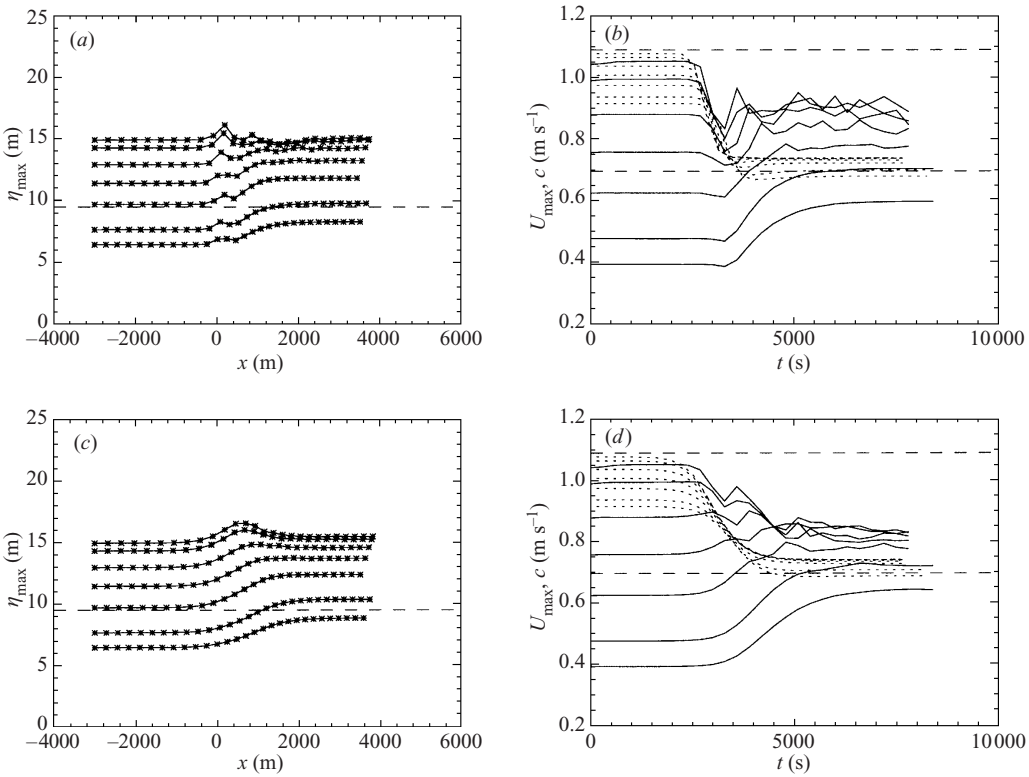

FIGURE 11. Evolution of wave properties for various initial waves using exponential stratification with $S = 15$ m. (*a*) Maximum downward isopycnal displacement as function of position of maximum displacement for narrow shelf $L = 200$ m. Stars indicate plotted values at 300 s intervals. Dashed line indicates breaking amplitude in shallow water. (*b*) Evolution of maximum horizontal velocity (solid) and propagation speed of leading wave (dotted) plotted as functions of time. Narrow shelf $L = 200$ m. Dashed lines indicate propagation speed at breaking limit in deep water (upper dashed line) and shallow water (lower dashed line). (*c*, *d*) As in (*a*) and (*b*) but for wider shelf $L = 600$ m.

did not occur either. Overturning could occur at the bottom, particularly for cases with large scale heights. This occurred as dense fluid pushed up the slope receded back down the slope.

The plots of maximum horizontal velocity and wave propagation speeds include dashed lines indicating the wave propagation speed at the breaking amplitude (c_{br}) in the deep and shallow water. For cases with final amplitudes above the breaking amplitude, the maximum velocity in the wave is larger than the wave propagation speed, both being greater than c_{br}. For waves with final amplitudes below the breaking amplitude, the maximum velocity is less than the propagation speed, both being lower than c_{br}.

The results also show that U_{max} depends on the shelf-slope width. The largest final values for $S = 15$ m occur for the narrow shelf slope, whereas for $S = 35$ m the largest occur for the wide shelf slope. This can be more easily seen in figure 2(*d*), where average values obtained using shelf-slope widths of 200 and 600 m are plotted using different symbols. This shows that the details of the flow in the wave core depend on the shelf-slope width. The wave propagation speed appears to be independent of the shelf-slope width and increases slightly more slowly, as a function of wave amplitude, than c does for the convectively unstable solitary waves. The maximum

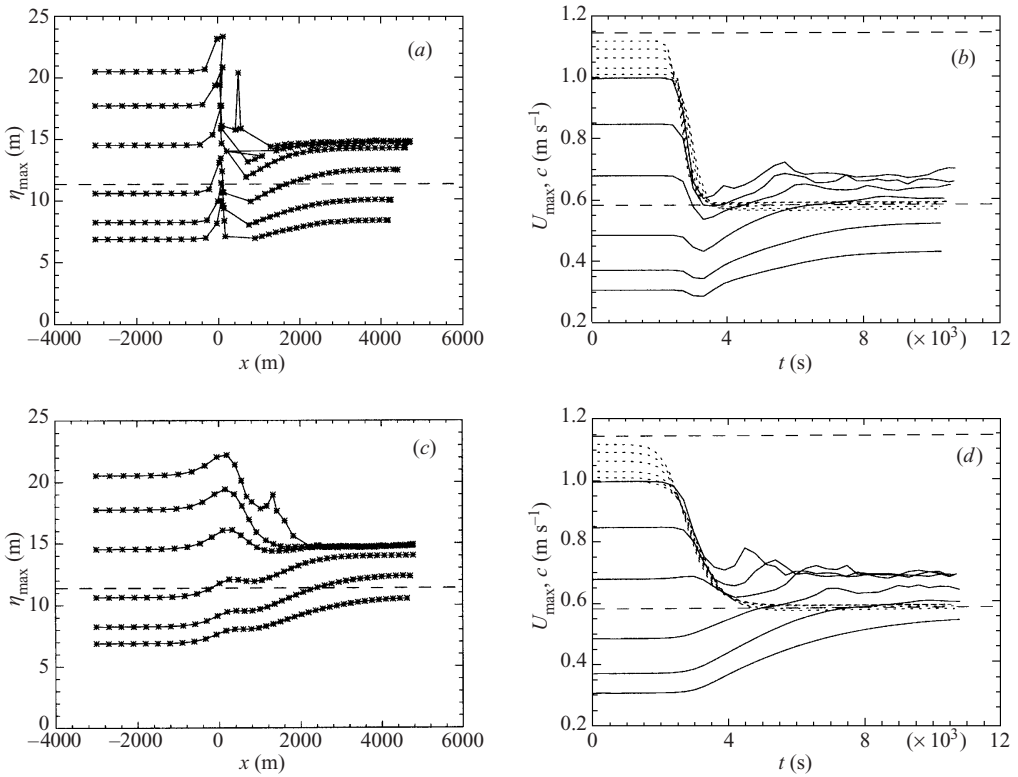

FIGURE 12. As in figure 11 but for density scale height $S = 35$ m.

horizontal velocity for the shoaled waves increases more rapidly than c, at a rate much less than does U_{max} for the convectively unstable solitary waves. Because the fluid in the convectively unstable core is circulating in the opposite sense to that in the cores of shoaled waves, the large difference is not surprising. For nearly linear stratifications, Derzho & Grimshaw (1997) predicted that to leading order the fluid in a wave core is stagnant. While the present results do not show this, there is some qualitative similarity in the sense that the theory predicts a sharp reduction in the rate of increase of U_{max}. The present results agree with the prediction of Derzho & Grimshaw (1997) that the c vs. amplitude curve flattens out at large amplitudes.

Figure 13 shows the results for the exponential densities with $S = 75$ m for a shelf-slope width $L = 600$ m. These runs used a lower horizontal resolution ($\delta x = 10/3$ m) because longer computational domains were required. The time scale of wave evolution is increased so much that even with the reduced propagation speeds a longer shallow-water region is required to allow the shoaled wave to evolve to a final form. For the smaller-amplitude cases a final form has not been reached and runs were discontinued when breaking occurred or the wave reached the boundary. A maximum amplitude of 14.1 m for the shoaled waves is attained for the three largest initial waves. Results obtained using density $\bar{\rho}_2$ for $S = 20$ and 45 m are qualitatively similar to those obtained for density $\bar{\rho}_1$ (not shown).

In figure 14 the evolution of waves using the mixed-layer stratification and the narrow shelf are shown. The results are quite different than for the exponential stratification. All waves have a final amplitude below the conjugate flow amplitude, indicated by the dashed line in figure 14(a). In figure 14(b) the dashed lines indicate the

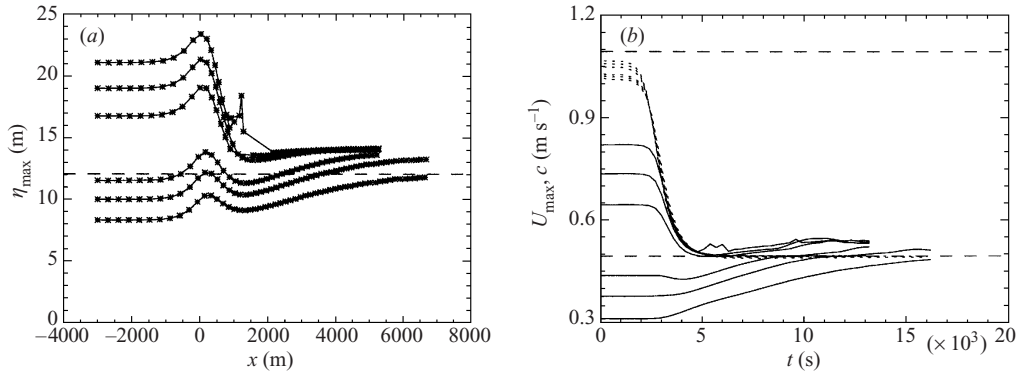

FIGURE 13. As in figure 11 but for density scale height $S = 75$ m. Wide shelf topography $L = 600$ m only.

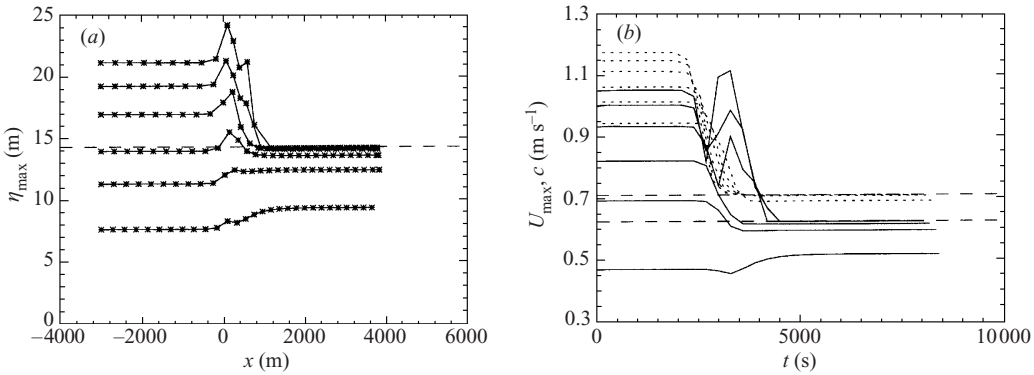

FIGURE 14. As in figure 11 but for mixed-layer stratification. Narrow shelf topography $L = 200$ m only. Dashed lines in (*b*) are propagation speed (upper) and maximum horizontal velocity (lower) of shallow water conjugate flow.

propagation speed and maximum horizontal velocity of the shallow-water conjugate flow. For all final waves, $U_{max} < c$ with both values being less than or equal to the corresponding values for the conjugate flow. This illustrates the result that none of the shoaled waves have trapped cores. The three largest initial waves, having amplitudes $\geqslant 16.9$ m, form final on-shelf waves with η_{max}, U_{max} and c equal to the corresponding conjugate flow values.

5.2. *Breaking depths*

In figure 15 some data on the locations of initial wave breaking are plotted. Shown are the water depth, horizontal location and distance below the surface of the first occurrence of a density inversion in the upper half of the computational grid. Only these grid points were considered in order to focus on overturning in the shoaling wave rather than near bottom overturning. Results from the exponential stratifications with $S = 15$ and 35 m and for the mixed-layer stratification are presented for three shelf-slope widths, $L = 200$, 400 and 600 m.

Consider first the exponential stratification with $S = 15$ m (first column). Waves with initial amplitudes $\leqslant 15.31$ m were considered. At this amplitude $U_{max}/c \approx 0.99$, indicating that the initial wave is very close to breaking. Runs with larger initial waves showed a rapid increase in the breaking depth; however the results were sensitive to

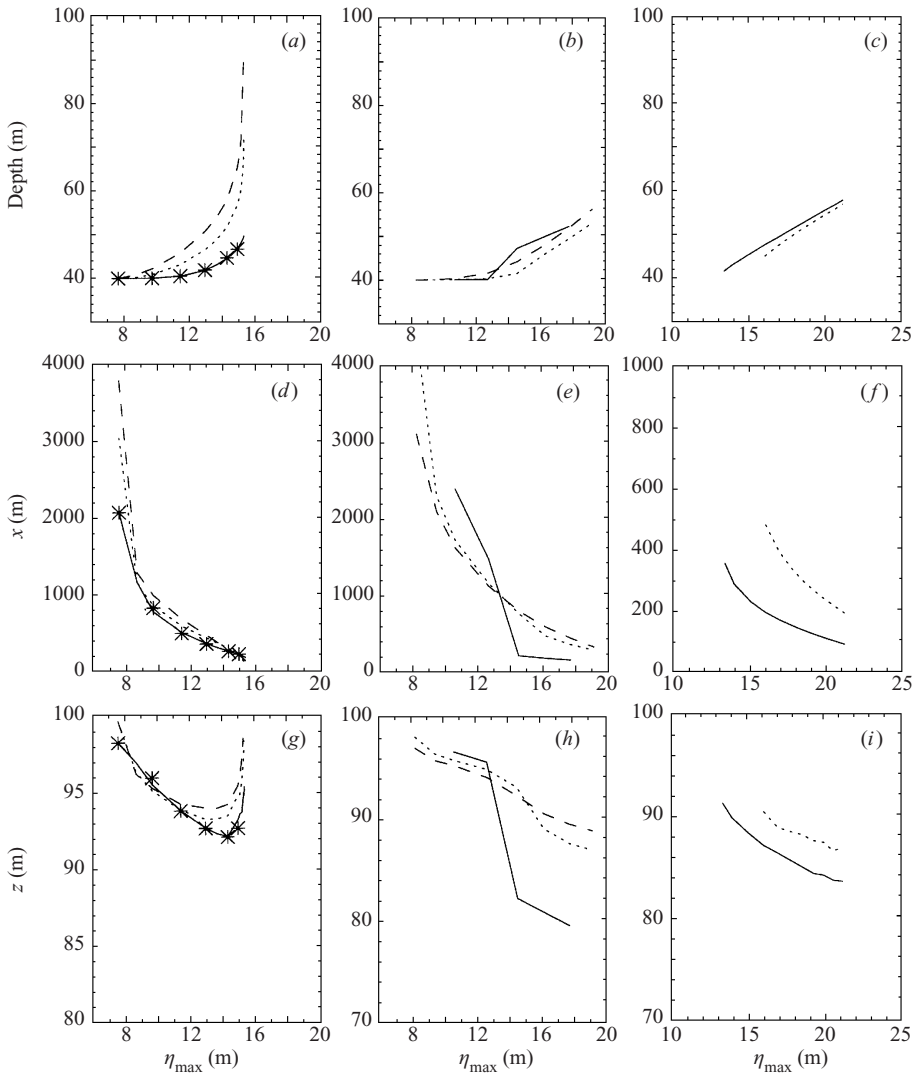

FIGURE 15. Location of first breaking for three different shelf widths: $L = 200$ m (solid), 400 m (dotted) and 600 m (dashed). (a, d, e) Exponential stratification with $S = 15$ m. (b, e, h) exponential stratification with $S = 35$ m. (c, f, i) Mixed-layer stratification. Shown are water depth when overturning first occurs (a, b, c), horizontal position of first overturning (d, e, f) and height of first overturning (g, h, i). Only overturning in upper half of computational grid was considered. For exponential stratifications with $S = 35$ m sudden change in values for η larger than 12 m (solid curve) and for η larger than 15 m (dotted curve) is due to breaking occurring at bottom of upper half of the computational domain rather than in the leading wave. See text.

the numerical resolution. Increasing L increases the depths at which the waves break. The minimum initial wave amplitude for which breaking occurs is approximately 7.4 m. It decreases slightly as L increases (this cannot be seen in the figure). For small-amplitude waves, breaking occurs well onto the shelf (figure 15*d*) near the surface (figure 15*g*). This is expected, since, at the breaking amplitude $U_{max} = c$ at the surface for the exponential stratification. As the initial wave amplitude is increased breaking occurs earlier and further below the surface. For very large waves the water

depth at which breaking first occurs increases rapidly and breaking occurs closer to the surface. This is because the initial wave is close to the breaking amplitude. Note that initial wave breaking occurs at different distances below the surface for different shelf-slope widths, an indication that the shelf-slope width plays a role in determining the fluid density in the core. This may be responsible for the different values of $U_{\max}$ in wave cores obtained using different shelf-slope widths (see figure 2).

For the exponential stratification with $S = 35$ m (figure 15, second column) breaking for large waves occurs first near the bottom and then progressively along a sloping line extending from the bottom up to the surface. In these cases, the breaking location is at the bottom of the top half of the computational grid and not necessarily in the leading wave. Indeed, as the shoaling wave has not formed an isolated solitary wave in the shallow water at that time it is difficult, if not meaningless, to determine when breaking first occurs in the wave. In figures 15(b, e, h) the sudden upward jump in the breaking depth and downward jump in x and z for cases with $L = 200$ at $\eta_{\max} \approx 14$ m are indicative of this phenomenon. This effect becomes less pronounced, and occurs at larger initial wave amplitudes, as the shelf-slope width increases. For small initial waves, trends are similar to those for $S = 15$ m.

For the mixed-layer stratification the dependence of the breaking depth on L is quite different. Increasing L decreases the depth at which the wave breaks and increases the minimum wave amplitude for which breaking occurs. For $L = 600$ m overturning in the solitary wave did not occur.

For the exponential stratification, for which solitary wave amplitudes are limited by the breaking limit, wider slopes and the resulting increase in energy in the leading wave results in a greater tendency for these waves to break as they shoal. Hence, smaller initial waves break for larger L. The breaking depth increases as L increases (figure 15a) since for depths less than 70 m (i.e. beyond the centre of the shelf slope at $x = 0$), the time a wave spends over the shelf slope before it arrives at a specified depth increases with L. Hence, the larger L is, the larger the wave is at a given depth both because the wave has had more time to adjust to its local environment, and also because of greater energy in the leading wave. Since waves are amplitude limited by the breaking limit in all depths, the result is that breaking first occurs in greater depths as L is increased.

For the mixed-layer stratification, shallow water waves are limited in amplitude by the conjugate flow limit. Thus, these waves are trying to deform to non-breaking waves as they shoal. Wider slopes give them more time to adjust, hence the minimum wave amplitude for which breaking occurs increases with L. Waves propagate further and into shallower water before they break, and for $L = 600$ wave breaking is completely counteracted by this adjustment.

5.3. *Properties of waves with trapped cores*

For the exponential and hyperbolic tangent density profiles, waves which break form a wave with a trapped, recirculating core of fluid which provides a very effective means of transporting a parcel of fluid great distances. As shown in figures 11–13, all waves with a trapped core propagate faster than the propagation speed of a wave at the breaking limit.

Consider the case shown in figure 5 (exponential density with $S = 15$ m, initial amplitude 14.3 m). A close-up of the wave core is given in figure 16 where contour plots of the density, velocity and the vorticity ($u_z - w_x$) fields are presented for two different times. At $t = 80$ min, shortly after the wave has broken, a tongue of relatively light fluid can be seen extending below the core. Most of the fluid in the tongue rises

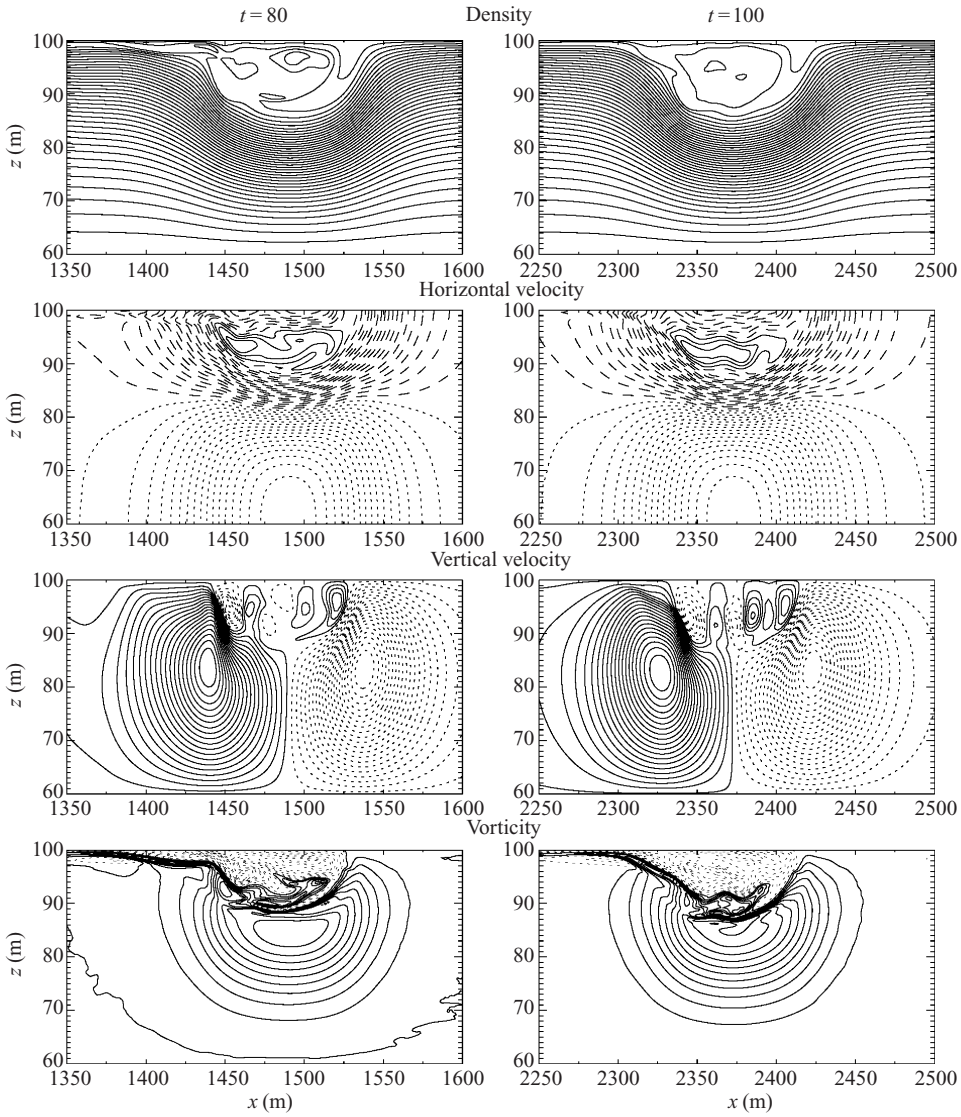

FIGURE 16. Contour plots of a solitary-like wave with a recirculating core. Exponential stratification with $S = 15\,\mathrm{m}$, $L = 200$ and initial amplitude 14.3 m (same case as shown in figure 5). For horizontal velocity contour plots the solid curves are values greater than the wave propagation speed $c = 0.73\,\mathrm{m\,s^{-1}}$, dashed are positive values less than c, and dotted curves are negative values. For vertical velocity contour plots solid/dotted curves are positive/negative values.

immediately ahead of the core. Some passes under the core and rises more slowly behind it. This is indicated by the positive w contours near the surface at about $x = 1520\,\mathrm{m}$ and the smaller positive values extending up to the surface at about $x = 1470\,\mathrm{m}$. The positive w values just below the surface at $x = 1500\,\mathrm{m}$ are for the rising fluid in the core. At $t = 100\,\mathrm{min}$ the large tongue is no longer apparent. A small depression in the isopycnal nearest the surface can be seen just ahead of the core. This feature grows until a new tongue of near-surface fluid passes under the core at which point it is pinched off, illustrating the unsteady nature of the core. There is also an indication of some small overturning features at the rear of the wave. Note

also that light surface fluid passes over the core. The vertical velocities at $t = 100$ show two peaks in upward motion near the surface at about $x = 2405$ and 2385 m. The first of these is associated with the upwelling at the back of the small surface depression ahead of the core. The second is associated with the fluid motion in the core itself.

The motion in the core has the form of two counter-rotating vortices. In the upper 8 m (approximately) of the core the vorticity is negative (counter-clockwise). Below, the vorticity is positive right down to the bottom boundary. Just below the region of negative vorticity is a small, highly contorted, patch of strong positive vorticity. Part of it lies inside the core, as is most readily apparent at $t = 100$ min where some of it can be seen to lie inside the closed density contour. Examination of individual particle paths confirms this (not shown). The negative vorticity is created as the wave overturns at the back. In an exact solitary wave propagating in fluid of constant depth, the flow is symmetric about the centreline. For waves of depression propagating to the right, as considered here, positive vorticity is created as fluid enters the wave where the baroclinic generation term $g\rho_x$ is positive. The vorticity of a fluid particle reaches its maximum when it reaches the centre of the wave. In the back half of the wave $g\rho_x$ is negative and, by symmetry, the vorticity of a fluid particle decreases to zero as it leaves the wave. As a wave shoals its rear steepens. The baroclinic generation of negative vorticity is enhanced and waves leave the rear of the wave with negative vorticity. This is particularly pronounced near the surface as these fluid particles have spent more time in the region of strong negative vorticity generation. In tandem with the flux of fluid with negative vorticity out of the back of the wave, waves are shed. When the wave overturns at the back there is strong negative vorticity generation. As the tongue of fluid falls forward and down, positive vorticity is generated underneath it. In figure 16 the bottom of the region of negative vorticity is centred on the patch of fluid with $u > c$ which lies between 5 and 10 m below the surface. At the front of it are positive vertical velocities and at the surface there is a local velocity minimum. At $t = 100$ min the surface velocity maximum is about 0.7 m s^{-1} ahead of the core. It drops to 0.5 m s^{-1} above the core and then increases again to 0.6 m s^{-1}, before monotonically decreasing to zero behind the wave (see figure 9*c*). The dominant counter-clockwise flow in the core agrees with the results of Terez & Knio (1998); however it is in the opposite sense of those seen in laboratory exeriments and in atmospheric observations (Manasseh *et al.* 1998; Doviak & Christie 1989). This may be a consequence of the formation mechanism which in the latter two instances is associated with dense gravity currents, as suggested by Terez & Knio (1998).

Figure 17 shows a close-up of a wave core for a large-amplitude case using the exponential stratification with $S = 35$ m for $L = 200$ m. The initial wave amplitude was 20.5 m and the shoaled wave has attained the limiting amplitude of 14.8 m (see figure 12) and has a propagation speed of 0.59 m s^{-1}. Shoaled waves with trapped cores of limiting amplitude are broad with flat centres. This limiting amplitude behaviour of wave cores was predicted by Derzho & Grimshaw (1997). In the present simulations this behaviour occurs for stratifications with the large scale heights, i.e. for the stratifications most closely resembling those considered by Derzho & Grimshaw. Below the core the flow is nearly horizontally uniform apart from short waves superimposed on the main wave. These waves are most apparent near the lower boundary of the wave core and are presumably associated with instabilities in the high shear region at the bottom of the core where the Richardson number is less than 0.25. Inside the core the flow is more irregular. Shoaled waves with

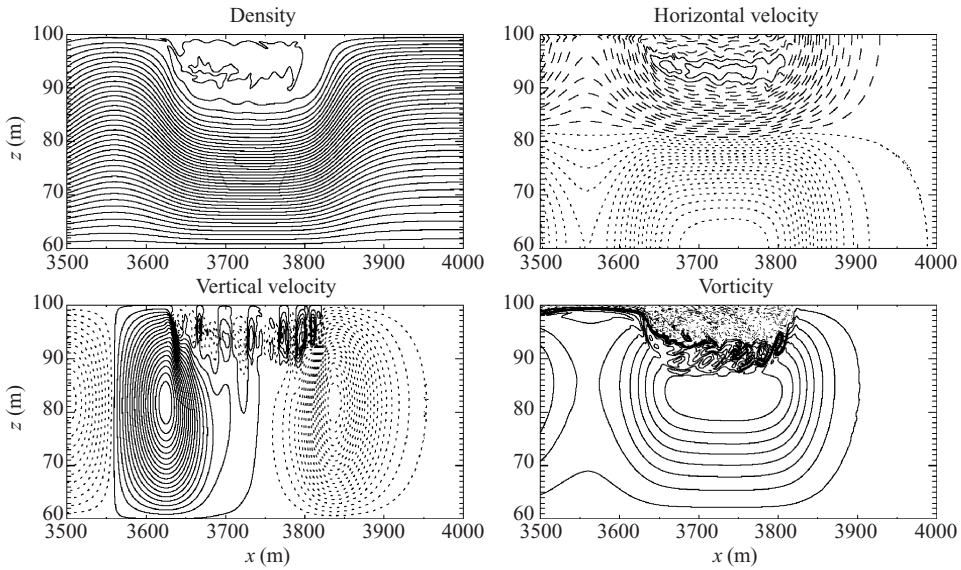

FIGURE 17. As in figure 16 but for wave with trapped core at limiting amplitude. Exponential stratification with $S = 35\,\mathrm{m}$, $L = 200\,\mathrm{m}$ and initial wave amplitude 20.5 m. Solid horizontal vorticity contours are for $u > c = 0.59\,\mathrm{m\,s^{-1}}$. $t = 150\,\mathrm{min}$.

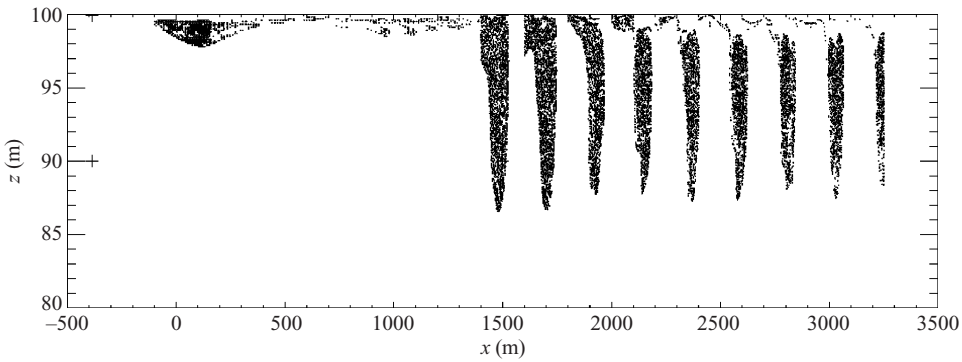

FIGURE 18. Particles in and around the recirculating core at times between 80 and 120 min (left to right), in 5 min intervals. Exponential stratification with $S = 15\,\mathrm{m}$, $L = 200$ and initial amplitude 14.3 m (same case as shown in figure 5). Particles with $x < 1400\,\mathrm{m}$ are the initial ($t = 0$) locations of the particles which are in and around the core at $t = 120\,\mathrm{min}$.

cores at the limiting amplitude for density $\bar{\rho}_2$ using $S = 45\,\mathrm{m}$ are also flat in the middle. The formation of flat-centred waves with trapped cores suggests that conjugate flows with closed streamlines may exist for monotonic stratifications, stratifications for which conjugate flows with open streamlines do not exist (Lamb & Wan 1998).

For the case depicted in figures 5 and 16, the motion of a dense field of 100 000 particles was monitored in order to determine where the water in the trapped core originated and to determine the size of the core. The particles were seeded over the top of the bank slope between $x = -500$ and 1500 m and between $z = 90.0$ m and the surface. Figure 18 shows the positions of the particles in and around the core at 5 minute intervals between $t = 80$ and 120 min. The figure was created by plotting

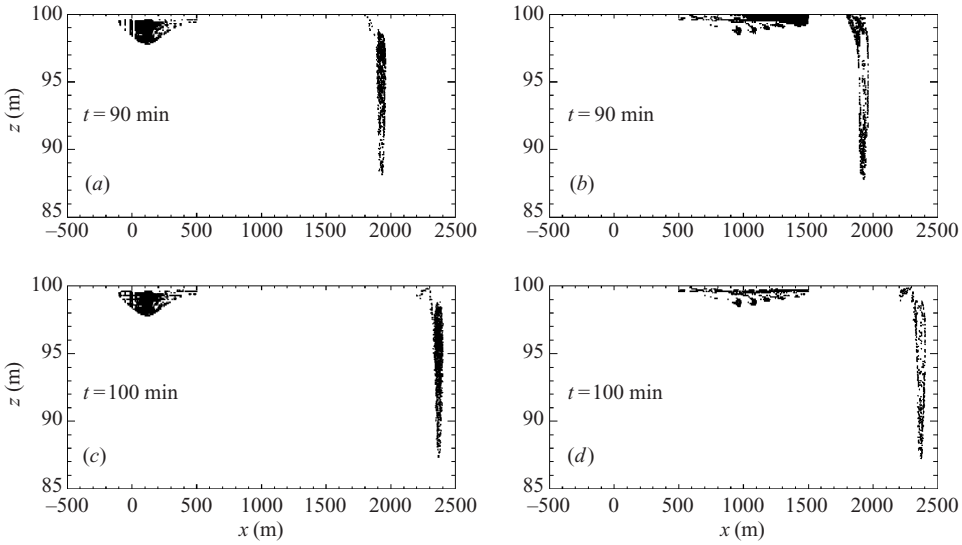

FIGURE 19. Particles in and around the core and their initial locations at $t = 90$ and $t = 100$ min. (a, c) Particles with initial horizontal coordinates less that 500 m; (b, d) Particles with initial horizontal coordinates greater that 500 m. Same case as figure 18.

the positions of particles whose x-coordinates are greater than a time-dependent specified value (for the first time, $t = 80$ min, only particles whose initial x-coordinate is less than 1300.0 are shown as the wave is still in the initial field of particles). Also plotted are the original positions of the particles that are in and around the core at $t = 120$ min. There are two sources of these particles. The first is a roughly triangular region lying in the upper 2.5 m between about $x = -100$ m and $x = 350$ m. The second source is spread over a region between $x \approx 400$ m and $x = 1500$ m. The first of these are the particles in the fluid that plunges into the depression when the core is formed. The second set are particles which, in the early stages of the formation of the core, are in the light fluid ahead and below the forward plunging fluid, and so are perhaps more accurately described as being wrapped around the core. The first few groups of particles shown in figure 18 have many more such particles. Note that the maximum depth of the particles oscillates in time. This illustrates the non-steady nature of the wave over this time interval.

In figure 19 the positions of particles in and around the wave core, along with their initial locations, are plotted by splitting them into two groups. The two groups are those with initial x-coordinates less than and greater than 500.0 m. These correspond, approximately, to particles in and around the core respectively. At $t = 90$ min one can clearly see that, in general, the particles with initial x-coordinates less than 500 m are inside the core while those with initial x-coordinates greater than 500.0 m are wrapped around the core. At $t = 100$ min the number of particles originating from $x > 500.0$ m is greatly reduced while the number originating from $x < 500$ m has not significantly changed.

In contrast, for the case presented in figure 12, for which a wave with a trapped core was not formed, no particles remain in the lead wave at $t = 120$ min. The maximum transport distance of a particle was approximately 1540 m for a particle whose initial location was 1 m below the surface at $x \approx 1160$ m.

In figure 20 vertical profiles of the horizontal velocity, density and the steady

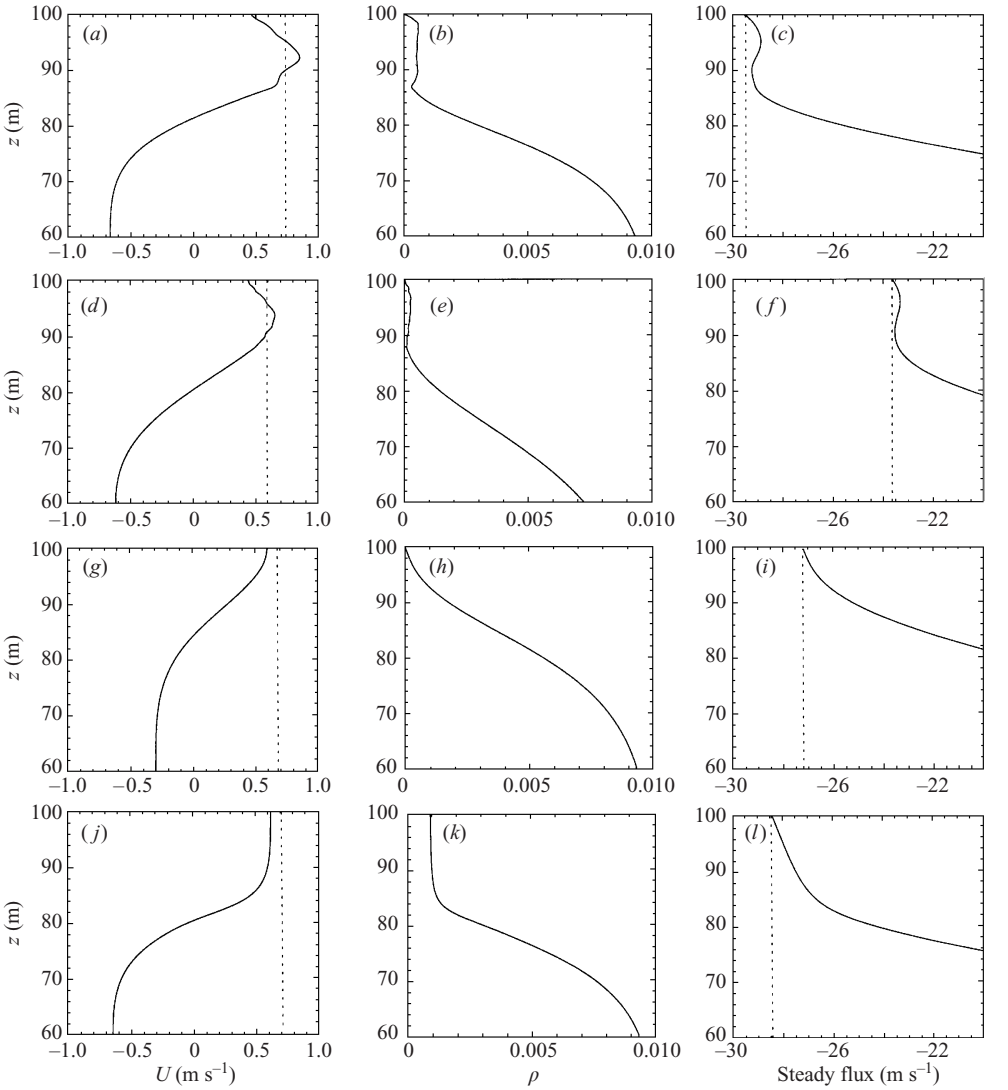

FIGURE 20. Vertical profiles of horizontal velocity (first column), density (second column) and steady volume flux (third column) through shoaled waves with trapped cores (*a–f*) and without trapped cores (*g–l*). (*a–c*) Exponential stratification with $S = 15$ m, $L = 200$ m, initial amplitude 14.3 m (core shown in figure 16). (*d–f*) Exponential stratification with $S = 35$ m, $L = 200$ m, initial amplitude 20.5 m (core shown in figure 17). (*g–i*) Exponential stratification with $S = 15$ m, $L = 200$ m, initial amplitude 6.4 m. (*j–l*) Mixed-layer stratification, $L = 200$ m, initial amplitude 21.2 m (shown in figure 10).

volume flux $f_s(z)$, defined by

$$f_s(z) = \int_{60}^{z} \big(u(x, z', t) - c\big)\, \mathrm{d}z', \tag{12}$$

are presented for the wave cores shown in figures 16 and 17 as well as for two cases without trapped cores. The steady volume flux is the volume flux between the bottom and height z in a reference frame moving with the wave. At the surface it has a value of $-cD$, where D is the water depth. This value is indicated by a vertical

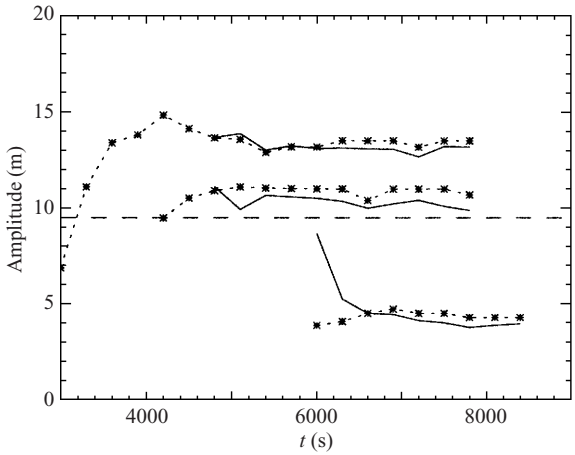

FIGURE 21. Comparison of core amplitudes as calculated using particles (solid) and using the occurrence of density inversion (dotted). Exponential density with $S = 15$ m using wide topography $L = 600$ m. Initial wave amplitudes are 7.6, 11.4 and 14.9 m. Core amplitudes increase with initial wave amplitude.

dotted line in figure 20. The value of x used for the profiles shown in figure 20 is the one at which the maximum downward isopycnal displacement in the wave occurs. The first of the cases without trapped cores is one using density $\bar{\rho}_1$ with $S = 15$ m, $L = 200$ m and an initial amplitude of 6.4 m. For this case wave breaking did not occur during shoaling. The second case is that presented in figure 12. This wave is in the mixed-layer stratification (initial amplitude 21.2 m) which is flat centred (i.e. at the conjugate flow amplitude).

The velocity profiles include a line indicating the wave propagation speed. For the two cases with cores, it can be seen that there is a thin subsurface region where the horizontal velocity exceeds the wave propagation speed c. Between this region and the surface the horizontal velocity is below the wave propagation speed and decreases with height. From the density profiles one can clearly see a subsurface layer in which the density is almost constant. For the first case a thin stratified layer overlying the core is clearly evident. The bottom of the core is below the height at which u first equals c. This is indicative of the presence of two counter-rotating vortices. For the cases without cores the horizontal velocity increases monotonically towards the surface and is always less than the wave propagation speed. The density and steady volume flux decrease monotonically with z.

Derzho & Grimshaw (1997) modelled a wave with a trapped core by using a separating streamline which left the surface ahead of the core and rejoined the surface behind the core. Streamlines were closed above the separating streamline and open beneath it. For such waves, the volume flux between the bottom and the separating streamline is independent of horizontal position and equal to $-cD$. Derzho & Grimshaw showed that to leading order the fluid is stagnant inside the core, in which case f_s would remain constant above the separating streamline. From figure 20(c,f) it is apparent that this is not the case in the present results. As z increases f_s decreases, reaches a local minimum which is greater than $-cD$, rises and then falls to $-cD$ at the surface. This shows that there is not a separating streamline that meets the surface and is indicative of near-surface fluid passing over the core. Flux profiles for every case looked at showed qualitatively similar behaviour.

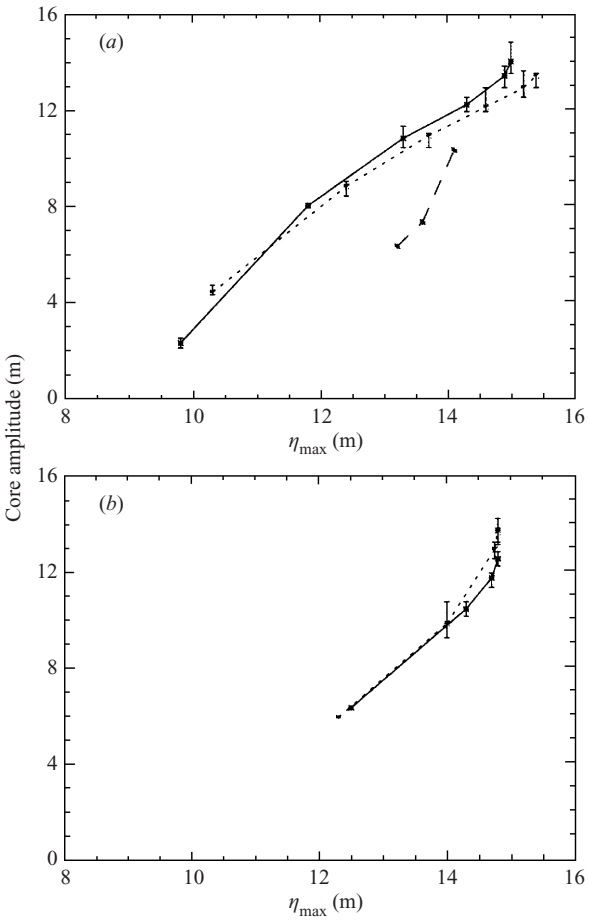

FIGURE 22. Core amplitudes as a function of final wave amplitude for exponential stratifications. (*a*) $S = 15$ m for shelf-slope widths of 200 m (solid) and 600 m (dotted) and for $S = 75$ m for a shelf-slope width of 600 m (dashed). (*b*) $S = 35$ m for shelf-slope widths of 200 m (solid) and 600 m (dotted). Core amplitudes are not steady in time. The error bars indicate range of values.

A couple of methods for determining the amplitude of the core have been considered. One is to use particle tracking. In this method (Terez & Knio 1998) the motion of a large number of particles is monitored and the core amplitude is defined as the maximum distance below the surface of a particle in the core. This is somewhat tedious so an alternative method is desirable. The second method is to use the greatest distance below the surface of a density overturn.

In figure 21 the core amplitudes, as determined using particles and density overturns, are compared for three different waves for the exponential density $\bar{\rho}_1$ with $S = 15$ m using the wide topography $L = 600$ m. Initial wave amplitudes were 7.6, 11.4 and 14.9 m. It can be seen that in all cases the two amplitudes are similar, with the amplitude based on density overturns being generally larger, in some cases by almost 1 m, a difference of approximately 10%. In figure 22 the core amplitudes (based on density overturns) are plotted as a function of the wave amplitudes for model runs using the exponential density with scale heights of 15, 35 and 75 m. Results for shelf-slope widths of $L = 200$ and 600 m are shown separately for the two smallest scale heights. For large waves, the core amplitudes are larger for the narrow shelf

Case	A	$\eta_{\max}$ (m)	L (m)	$M(0)$ (m^2)	Final $\%\Delta M$	$KE(0)$ ($m^4\,s^{-2}$)	Max $\%\Delta KE$	Final $\%\Delta KE$	Final $\%\Delta E$
S15L2c1	0.2	7.64	200	9.70	0.09	219.4	−8.0	−0.6	−0.8
S15L6c1	—	—	600	9.66	0.04	219.4	−3.2	−0.2	−0.2
S15L2c2	0.6	14.29	200	14.54	0.41	724.6	−8.0	−6.2	−1.0
S15L6c2	—	—	600	14.50	0.01	724.6	−6.1	−5.8	−1.1
modL2c1	0.3	9.65	200	11.09	0.09	340.0	−8.1	−3.7	−0.8
modL6c1	—	—	600	11.05	0.02	340.0	−4.3	−3.6	−0.8
modL2c2	1.5	21.17	200	22.58	1.69	1833.0	−14.1	−13.6	−2.1
modL6c2	—	—	600	22.54	0.10	1833.0	−13.3	−9.5	−0.5
S35L2c1	0.3	6.89	200	16.33	0.09	307.6	−28.1	−3.1	−1.5
S35L6c1	—	—	600	16.25	−0.40	307.8	−11.6	−1.3	−1.0
S35L2c2	1.0	14.53	200	24.98	0.30	1076.3	−23.1	−8.5	−5.2
S35L6c2	—	—	600	24.90	0.11	1076.3	−9.7	−3.8	−0.8

TABLE 1. Mass and energy changes during shoaling.

slope for $S = 15$ m whereas the core amplitudes are smaller for the narrow shelf slope when $S = 35$ m. The error bars on the plots indicate the variation of the core amplitude. For the $S = 75$ m cases error bars are not included. For these cases the waves were monotonically increasing except for the largest waves. Final values rather than averages have been plotted (see figure 13). The wave and core amplitudes increase as the incident solitary wave amplitude increases. While the wave amplitudes are almost constant in time (figure 11–14), core amplitudes show some variability, particular for the largest waves. These results are consistent with the suggestion by Terez & Knio (1998) that details of the wave structure do not have a pronounced effect on the large-scale motion of the wave.

6. Energetics

Energy conservation and energy distribution amongst the various waves present after a single solitary wave has shoaled is now considered. In the numerical method used, the model equations (1*a*)–(1*c*) are not cast in conservation form. Momentum is exactly conserved (to machine error) because the time derivative of the velocity field is written as a linear combination of divergence-free vectors; however mass and energy are not exactly conserved. A numerical instability which manifested itself in the deep water made it necessary to add some damping terms to the momentum and density equations when energetics are considered. The modified equations are

$$\boldsymbol{U}_t + \boldsymbol{U}\cdot\nabla\boldsymbol{U} = -\nabla p - \rho g\hat{\boldsymbol{k}} + (K_u\boldsymbol{U}_z)_z + M\boldsymbol{U}_{\chi\chi}, \tag{13a}$$

$$\rho_t + \boldsymbol{U}\cdot\nabla\rho = \left(K_\rho\rho_z\right)_z + M\rho_{\chi\chi}. \tag{13b}$$

Here χ is the horizontal terrain-following coordinate. Boundary conditions in the vertical are $u_z = \rho_z = 0$ along the top and bottom boundaries. The values of K_u, K_ρ and M are 7.5×10^{-4}, 1.0×10^{-6} and 2.5×10^{-3} $m^2\,s^{-1}$ in the deep water. They then decrease by a factor of 100 between about $x = -1050$ and -950 m. Thus, they are effectively zero in the shallow water. Comparisons of wave and core amplitudes, maximum velocity and propagation speeds for model runs with and without damping show only slight differences.

A total of twelve model runs were done using damping. These runs used the exponential stratification with $S = 15$ and 35 m and the mixed-layer stratification.

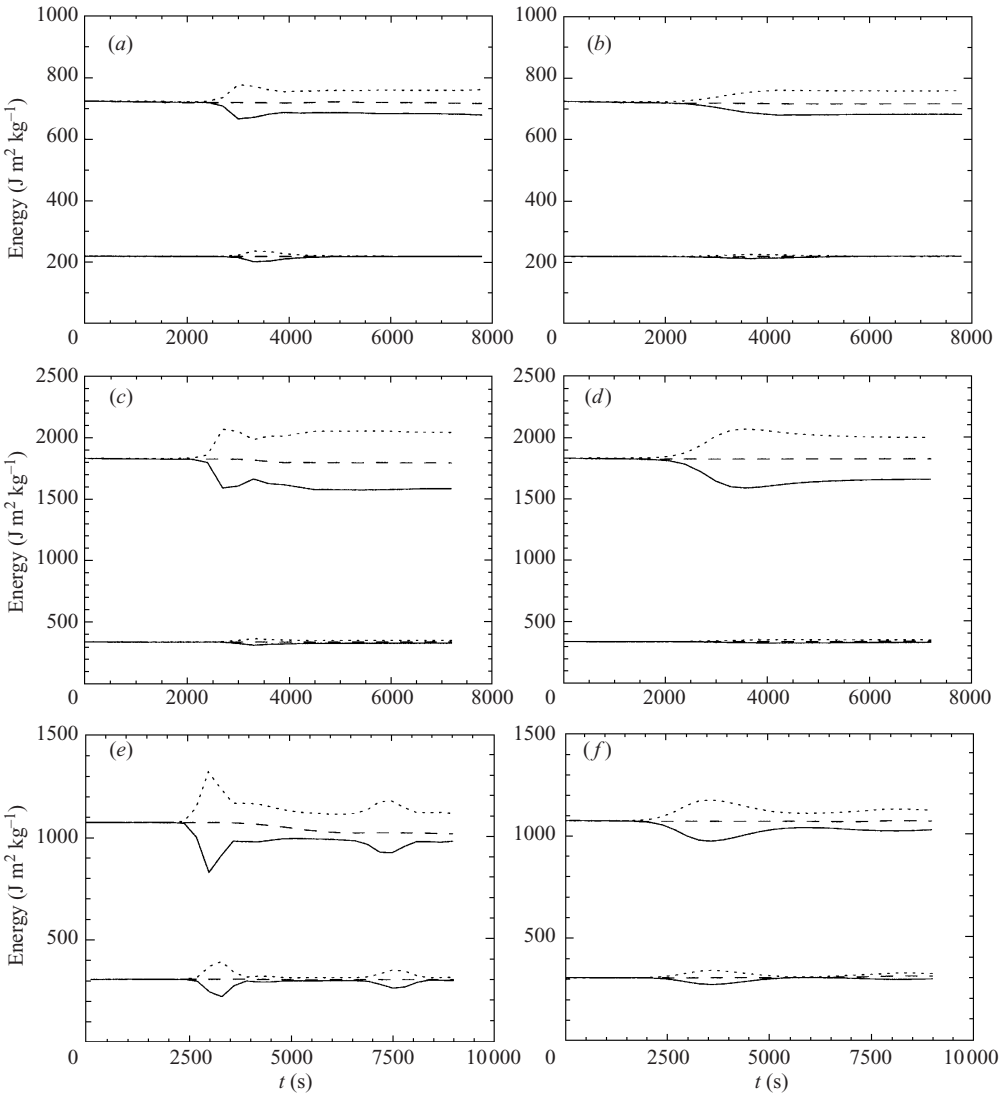

FIGURE 23. Time evolution of kinetic energy (solid curve), potential energy offset by initial kinetic energy (dotted curve), and total energy (dashed curve) for a shoaling wave using narrow shelf with $L = 200$ m (left column) and wide shelf with $L = 600$ m (right column). (a, b) Exponential stratification with $S = 15$ m for initial amplitudes of 7.6 and 14.3 m. (c, d) Mixed-layer stratification for initial amplitudes of 9.6 and 21.2 m. (e, f) Exponential stratification with $S = 35$ m for initial amplitudes of 6.9 and 14.5 m. (e) $L = 200$ m. (f) $L = 600$ m.

For each of these stratifications two initial wave amplitudes were used and each was run for shelf-slope widths of 200 and 600 m. For these runs the total kinetic and potential energy and the mass anomaly were monitored by integrating the appropriate fields over the computational domain ($-4000 \leqslant x \leqslant 4000$ m). The potential energy is defined so that its value is zero at $t = 0$. It is not the available potential energy, which is a function of the size of the computational domain. The mass anomaly $M(t)$ is defined as the negative of the integral of the density anomaly $\rho(x, z, t) - \bar{\rho}(z)$ over the computational domain. In table 1 the values of $M(0)$, the initial kinetic energy $KE(0)$,

Case	Time (min)	K_1 ($m^4 s^{-2}$)	$\%K_1$	$\%K_2$	$\%K_3$	$\%m_1$	$\%m_2$	% in $0 < x < m_2$	% in $x < 0$
S15L2c1	120	171.0	78.4	11.9	—	0.5	4.6	1.9	2.7
S15L6c1	—	192.6	87.6	9.1	—	0.2	1.8	0.6	0.7
S15L2c2	—	615.9	90.6	3.6	—	0.8	2.5	1.2	1.3
S15L6c2	—	655.6	96.1	2.2	—	0.1	0.7	0.4	0.4
modL2c1	—	285.3	87.9	4.9	—	0.4	3.9	1.5	1.3
modL6c1	—	308.1	94.3	3.1	—	0.2	1.3	0.5	0.5
modL2c2	—	1196.9	70.9	11.2	2.1	7.0	4.5	2.4	1.8
modL6c2	—	1574.7	95.0	2.3	—	—	1.8	0.5	0.4
S35L2c1	150	141.0	47.6	8.2	—	11.9	10.6	9.4	20.0
S35L6c1	—	197.6	64.9	14.6	—	4.1	6.5	3.9	6.0
S35L2c2	—	482	49.3	13.8	3.2	7.0	8.8	5.2	12.6
S35L6c2	—	829	79.1	6.4	1.0	3.4	4.1	2.6	3.4

TABLE 2. Kinetic energy distribution in the final wave field.

the maximum and final change of kinetic energy and the final change in total energy (kinetic plus potential) and the mass anomaly are given. The total energy does not decrease monotonically during a model run; however the maximum and final change in total energy are the same in all cases. For these runs the numerical model solved for the density anomaly rather than for the density. Recall that the density has been non-dimensionalized by a reference value, hence units of kg do not appear. For all but four cases, the final change in total energy is less than 1% and in all but one case the mass anomaly changes by less than 1% during the course of the model run. The largest changes in total energy (5.1%) occur for the large wave case using the exponential stratification with $S = 35$ m. For this case vigorous overturning between the surface and the bottom occurred (see figure 6).

Figure 23 shows the time evolution of the kinetic, potential and total energy for each of the 12 model runs. Here, for convenience, the potential energy has been offset by the initial value of the kinetic energy. As a solitary wave shoals the kinetic energy decreases and the potential energy rises so that the total energy is approximately conserved. Changes in kinetic energy at this stage are between 8% and 28% for the narrow topography and between 3% and 13% for the wide topography. For the small, non-breaking case using the exponential stratification with $S = 15$ m potential energy is converted back to kinetic energy as the wave adjusts to its new depth. After adjustment the percentage change in kinetic energy is less than 1%. For the other cases the final decrease in kinetic energy is an order of magnitude larger with a corresponding increase in potential energy. This includes the small-amplitude case for the mixed-layer stratification for which breaking did not occur during shoaling. For the cases using the exponential stratification with $S = 35$ m, a reflected wave is formed over the shelf slope. It propagates toward the deep water and reflects off the left boundary of the computational domain. During the reflection kinetic energy is converted to potential energy. This accounts for the increase in potential energy seen in figures 23(e,f) at about $t = 7500$ s.

In table 2 the kinetic energy distribution amongst various wave forms in the final wave field are given. K_1 is the kinetic energy in the leading wave while $\%K_1$, $\%K_2$, and $\%K_3$ give the percentage of the total kinetic energy in the three leading mode-one solitary waves, if present. Other values given are the percentage of the total kinetic energy: (i) in the mode-one wave train, lying between the mode-one solitary waves

and the mode-two solitary wave; (ii) in the mode-two solitary wave; (iii) lying between $x = 0$ and the mode-two solitary wave; and (iv) lying in the region $x < 0$. The latter is largely made up of energy in the reflected waves, although it may not account for all the reflected energy. For the cases using $S = 35$ m the percentage of kinetic energy was calculated using the total kinetic energy in the computational domain before the leftward propagating reflected wave reached the left boundary. In all cases the amount of energy in the leading wave is substantially higher, and the energy in the reflected waves ($x < 0$) is substantially lower, for runs using the wide shelf than for the corresponding model runs using the narrow shelf.

7. Summary and conclusions

The evolution of shoaling solitary internal waves, with a focus on the formation of solitary waves with trapped cores, has been investigated using a two-dimensional numerical model. The model was initialized with a single solitary wave in water 100 m deep. The wave subsequently propagates into shallow water 40 m deep. It was found that waves with trapped cores are easily formed in density fields for which the buoyancy frequency increases monotonically towards the surface (monotonic stratifications). Two such density fields, given by exponential and hyperbolic tangent profiles, were considered. The emphasis was on the exponential stratification for which three different scale heights were used.

One of the exponential stratifications was modified by introducing an upper mixed layer approximately 2 m thick, 5% of the shallow water depth. This was found to significantly modify the shoaling behaviour of the waves, completely eliminating the formation of waves with trapped cores. This result can be understood from a consideration of limiting wave amplitudes. For the monotonic stratifications, waves with open streamlines (in a reference frame moving with the wave) are limited in amplitude by the breaking limit, at which point the maximum horizontal velocity $U_{\max}$ is equal to the wave propagation speed c. For the mixed-layer stratification, waves in the shallow water are limited in amplitude by the conjugate flow limit for which $U_{\max}/c = 0.879$. Large-amplitude waves in shallow water thus evolve to waves far from breaking. It is conjectured that waves with trapped cores will not be formed if conjugate flows with open streamlines exist. This has been confirmed using several other stratifications. This ongoing work will be reported elsewhere.

These results have significant implications, as they imply that waves with trapped cores will not be formed in the ocean under most oceanographic conditions. Only at special locations or times, when the upper mixed layer is exceedingly thin, will waves with trapped cores possibly be formed. The sensitivity of the results to the near-surface stratification demonstrates the need to take measurements close to the surface. For example, solitary waves have been computed using a stratification based on density measurements taken off the coast of La Jolla, California in water 28 m deep (C. Lennert-Cody, personal communication). Density measurements were taken to within 0.5 m of the surface. Calculations done by the author show that in some cases solitary waves are limited by the breaking limit if the buoyancy frequency is linearly extrapolated to the surface but is limited by the conjugate flow limit if the buoyancy frequency is decreased more rapidly. Thus, this is one example of a location where waves with trapped cores may be formed at certain times. It is also possible that the presence of a background flow with sufficiently strong near-surface vorticity would allow waves with trapped cores to be formed.

For all stratifications considered solitary waves are waves of depression. Shoaling

waves increase in amplitude as they pass over the shelf slope, typically attaining their peak amplitude over the upper half of the shelf slope. They become asymmetric during shoaling, being steeper at the rear of the wave where overturning may occur for sufficiently large waves. Eventually the wave field is composed of a large leading solitary wave followed by one or two smaller solitary waves (usually one). Trailing these are a mode-one wave train, a mode-two wave and other higher-mode waves. Reflected waves are also formed.

For the monotonic stratifications, if overturning occurs at the rear of the wave the forward plunging fluid fills the wave and an unsteady solitary-like wave with a trapped fluid core is formed in the shallow water. The shoaling wave may arrive in shallow water before breaking has occurred. For the shelf slopes considered here the wave has not had time to completely adjust to the new depth and it continues to evolve after it has reached the shallow water. As it evolves to a final form it grows in amplitude and in so doing may exceed the breaking amplitude. Hence, waves may overturn and form waves with trapped cores well onto the shelf. This behaviour becomes more pronounced as the scale height for the stratification increases, as this increases the evolution time scale of the waves. This effect dominates the reduced propagation speeds so that waves must propagate greater distances to reach a final form. This makes model runs using stratifications with large scale heights difficult. Waves with trapped cores have propagation speeds, maximum currents, and amplitudes which are larger than the corresponding values for the largest non-breaking wave in the shallow water. The fluid in the core has two counter-rotating vortices. The upper one is the larger and has negative vorticity $u_z - w_x$, i.e. it circulates counter-clockwise, rising at the front of the core (waves are propagating rightward). A wider shelf slope results in larger leading solitary waves in the shallow water and the critical initial wave amplitude, η_{crit}, above which shoaling waves break, decreases as the topographic slope decreases. All breaking waves formed a core, even those with initial amplitudes only slightly above η_{crit}. Indeed, the presence of a recirculating core was often the only indication that breaking had occurred.

Maximum currents in waves with trapped cores were found to depend on the shelf width and hence on the details of the formation of the core. For the exponential densities with scale heights of 35 and 75 m, and for the hyperbolic tangent density with a scale height of 45 m, waves with trapped cores were limited in amplitude. Waves at the limiting amplitude were flat in the middle, suggesting the existence of conjugate flows with closed streamlines. The limiting amplitude depends slightly on the shelf-slope width.

The flow in the wave cores is variable, as shown by variations in the maximum horizontal velocity in the core and in the core amplitude. The variability increases as the resolution increases, suggesting that at a much higher resolution the recirculating core would have more structure and be more dynamically active. Three-dimensional effects would probably substantially modify the flow in the wave core with possibly little effect on the flow outside the core. This warrants investigation. Three-dimensional effects could also significantly modify the wave field that evolves from regions of strong overturning behind the leading wave.

Many of the properties of the waves with wave cores are similar to those predicted by Derzho & Grimshaw (1997) in spite of the fact that the stratifications considered here do not have nearly constant buoyancy frequency. Similarities include a flattening of the propagation vs. amplitude curve compared with convectively unstable waves computed by the solitary wave solver, and the existence of a limiting amplitude for waves with cores. The limiting amplitude was found for stratifications with the largest

scale heights considered, i.e. for those most closely resembling the stratifications considered by Derzho & Grimshaw. There is some indication that wave properties outside the core are not sensitive to the flow inside the core, as found by Terez & Knio (1998).

When the exponential density with a scale height $S = 15$ m is modified to include a 2 m thick upper mixed layer, solitary wave amplitudes are limited by the stability limit in deep water and by the conjugate flow limit in shallow water. Wave breaking only occurred over the shelf slope. If the leading solitary wave arrived on the shelf before breaking then, as it continued to adjust to shallow water, it could not exceed the conjugate flow amplitude. Hence the maximum horizontal velocity in the wave always stayed well below the wave propagation speed and no overturning would occur in the shallow water. A few model runs using the exponential stratification ($S = 15$ m) modified to have surface mixed layers 5 and 10 m thick have also been done. The results were qualitatively similar to those presented for the 2 m mixed-layer case. For the mixed-layer stratification, because the overturning is restricted to the back of the shoaling solitary wave, three-dimensional effects are not expected to significantly modify the leading wave.

This work was funded by a grant from the Natural Sciences and Engineering Research Council of Canada. Some of the model results presented herein were obtained using an NEC SX5, time on which was generously provided by R. Peltier.

REFERENCES

Akylas, T. R. & Grimshaw, R. H. J. 1992 Solitary internal waves with oscillatory tails. *J. Fluid Mech.* **242**, 279–298.

Bell, J. B., Colella, P. & Glaz, J. M. 1989 A second-order projection method for the incompressible Navier-Stokes equations. *J. Comput. Phys.* **85**, 257–283.

Bell, J. B. & Marcus, D. L. 1992 A second-order projection method for variable-density flows. *J. Comput. Phys.* **101**, 334–348.

Benjamin, T. B. 1966 Internal waves of finite amplitude and permanent form. *J. Fluid Mech.* **25**, 241–270.

Boussinesq, J. 1872 Théorie des ondes des remous qui se propagent le long d'un rectangulaire horizontal, en communiquant au liquide contenu dans ce canal des vitesses sensiblement pareilles de la surface au fond. *J. Math. Pures Appl.* **17**, 55–108.

Brown, D. J. & Christie, D. R. 1998 Fully nonlinear solitary waves in continuously stratified incompressible boussinesq fluids. *Phys. Fluids* **10**, 2569–2586.

Cacchione, D. & Wunsch, C. 1974 Experimental study of internal waves over a slope. *J. Fluid Mech.* **66**, 223–239.

Cheung, T. K. & Little, C. G. 1990 Meteorological tower, microbarograph array, and sodar observations of solitary-like waves in the nocturnal boundary layer. *J. Atmos. Sci.* **47**, 2516–2536.

Christie, D. R. 1992 The morning glory of the Gulf of Carpentaria: a paradigm for non-linear waves in the lower atmosphere. *Austral. Met. Mag.* **41**, 21–60.

Clarke, R. H., Smith, R. K. & Reid, D. G. 1981 The Morning Glory of the Gulf of Carpentaria: An atmospheric undular bore. *Mon. Weath. Rev.* **109**, 1726–1750

Clarke, S. R. & Grimshaw, R. H. J. 1999 The effect of weak shear on finite-amplitude internal solitary waves. *J. Fluid Mech.* **395**, 125–159.

Davis, R. E. & Acrivos, A. 1967 Solitary internal waves in deep water. *J. Fluid Mech.* **29**, 593–607.

Derzho, D. J. & Grimshaw, R. 1997 Solitary waves with a vortex core in a shallow layer of stratified fluid. *Phys. Fluids* **9**, 3378–3385.

Djordjevic, V. D. & Redekopp, L. G. 1978 The fission and disintegration of internal solitary waves moving over two-dimensional topography. *J. Phys. Oceanogr.* **8**, 1016–1024.

Doviak, R. J. & Christie, D. R. 1989 Thunderstorm-generated solitary waves: a wind shear hazard. *J. Aircraft* **26**, 423–431.

Green, G. 1837 On the motion of waves in a variable canal of small depth and width. *Camb. Trans.* **VI** (Papers p. 225).

Grimshaw, R. 1970 The solitary wave in water of variable depth. *J. Fluid Mech.* **42**, 639–656.

Grimshaw, R. 1983 Solitary waves in density stratified fluids. In *Nonlinear Deformation Waves. Proc. IUTAM Sym. Tallinn* (ed. V. Nigul & J. Engelbrecht), pp. 431–447.

Grue, F., Jensen, A., RusÅs, P.-O. & Sveen, J. K. 2000 Breaking and broadening of internal solitary waves. *J. Fluid Mech.* **413**, 181–217.

Hazel, P. 1972 Numerical studies of the stability of inviscid stratified shear flows. *J. Fluid Mech.* **51**, 39–61.

Helfrich, K. R. 1992 Internal solitary wave breaking and run-up on a uniform slope. *J. Fluid Mech.* **243**, 133–154

Helfrich. K. R. & Melville, W. K. 1986 On long nonlinear internal waves over slope-shelf topography. *J. Fluid Mech.* **167**, 285–308.

Holloway, P. E., Pelinovsky, E., Talipova, T. & Barnes, B. 1997 A nonlinear model of internal tide transformation on the Australian North West Shelf. *J. Phys. Oceanogr.* **27**, 871–896.

Howard, L. N. 1961 Note on a paper of John W. Miles. *J. Fluid Mech.* **10**, 509–512.

Huthnance, J. M. 1989 Internal tides and waves near the continental shelf edge. *Geophys. Astrophys. Fluid Dyn.* **48**, 81–105.

Ivey, G. N. & Nokes, R. I. 1989 Vertical mixing due to the breaking of critical internal waves on sloping boundaries. *J. Fluid Mech.* **204**, 479–500.

Johnson, R. S. 1973 On the development of a solitary wave over an uneven bottom. *Proc. Camb. Phil. Soc.* **73**, 183–203.

Johnson, R. S. 1994 Solitary wave, soliton and shelf evolution over variable depth. *J. Fluid Mech.* **276**, 125–138.

Kakutani, T. 1971 Effect of an uneven bottom on gravity waves. *J. Phys. Soc. Japan* **30**, 272–276 and 593.

Kamachi, M. & Honji, H. 1982 Steady flow patterns of internal solitary bulges in a stratified fluid. *Phys. Fluids* **25**, 119–1120.

Kao, T. W., Pan, F.-S. & Renouard, D. 1985 Internal solitons on the pycnocline: generation, propagation, and shoaling and breaking over a slope. *J. Fluid Mech.* **159**, 19–53.

Lamb, K. G. 1994 Numerical experiments of internal wave generation by strong tidal flow across a finite amplitude bank edge. *J. Geophys. Res.* **99**, 843–864.

Lamb, K. G. & Wan, B. 1998 Conjugate flows and flat solitary waves for a continuously stratified fluid. *Phys. Fluids* **10**, 2061–2079.

Manasseh, R., Ching, C.-Y. & Fernando, H. J. S. 1998 The transition from density-driven to wave-dominated isolated flows. *J. Fluid Mech.* **361**, 253–274.

Miles, J. W. 1961 On the stability of heterogeneous shear flows. *J. Fluid Mech.* **10**, 496–508.

Ostrovsky, L. A. & Stepanyants, Y. A. 1989 Do internal solitons exist in the ocean? *Rev. Geophys.* **27**, 293–310.

Saffarinia, K., & Kao, T. W. 1996 A numerical study of the breaking of an internal soliton and its interaction with a slope. *Dyn. Atmos. Oceans* **23**, 379–391.

Schmidt, N. P., & Spigel, R. H. 2000 Second mode internal solitary waves II – Internal circulation. In *Fifth Intl Symp. on Stratified Flows* (ed. G. A. Lawrence, R. Pieters & N. Yonemitsu), pp. 815–820.

Stamp, A. P. & Jacka, M. 1996 Deep-water internal solitary waves. *J. Fluid Mech.* **305**, 347–371.

Terez, D. E. & Knio, O. M. 1998 Numerical simulations of large-amplitude internal solitary waves. *J. Fluid Mech.* **362**, 53–82.

Tung, K.-K., Chan, T. F. & Kubota, T. 1982 Large amplitude internal waves of permanent form. *Stud. Appl. Maths* **66**, 1–44.

Turkington, B., Eydeland, A. & Wang, S. 1991 A computational method for solitary internal waves in a continuously stratified fluid. *Stud. Appl. Maths* **85**, 93–127.

Turner, R. E. L., & Vanden-broeck, J.-M. 1988 Broadening of interfacial solitary waves. *Phys. Fluids* **31**, 2486–2490.

Wallace, B. C. & Wilkinson, D. L. 1988 Run-up of internal waves on a gentle slope in a two-layered system. *J. Fluid Mech.* **191**, 419–442.